MICROSTRUCTURE, DIELECTRIC AND MAGNETIC PROPERTIES OF $Bi_{1-x}Gd_xMnO_3$ CERAMICS

A Dissertation Submitted to the Department of Physics, Bangladesh University of Engineering & Technology, Dhaka in Partial Fulfillment of Requirement for the Degree of Master of Philosophy in Physics

SUBMITTED BY

MD. SAIFUL ALAM

EXAMINATION ROLL NO.: 0413143003F

SESSION: April 2013

DEPARTMENT OF PHYSICS

BANGLADESH UNIVERSITY OF ENGINEERING & TECHNOLOGY

DHAKA 1000, BANGLADESH

CANDIDATE'S DECLARATION

It is hereby declared that this thesis or any part of it has not been submitted elsewhere for the award of any degree or diploma.
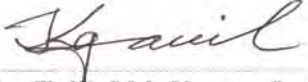
_____

MD. SAIFUL ALAM

BANGLADESH UNIVERSITY OF ENGINEERING & TECHNOLOGY (BUET), DHAKA
DEPARTMENT OF PHYSICS

CERTIFICATION OF THESIS

The thesis titled **"MICROSTRUCTURE, DIELECTRIC AND MAGNETIC PROPERTIES OF $Bi_{1-x}Gd_xMnO_3$ CERAMICS"** submitted by Md. Saiful Alam, Roll No-0413143003F, Registration No-0413143003F, Session: April-2013, has been accepted as satisfactory in partial fulfillment of the requirement for the degree of **Master of Philosophy** (M. Phil.) in Physics on 19 December, **2015**.

BOARD OF EXAMINERS

1.

Dr. Mohammed Abdul Basith   Chairman
Associate Professor   (Supervisor)
Department of Physics, BUET, Dhaka.

2.

Dr. Afia Begum   Member
Professor & Head   (Ex-Officio)
Department of Physics, BUET, Dhaka.

3.

Dr. Md. Abu Hashan Bhuiyan   Member
Professor
Department of Physics, BUET, Dhaka.

4.

Dr. Abu Talib Md. Kaosar Jamil   Member
Professor   (External)
Department of Physics
Dhaka University of Engineering and Technology, Gazipur.

DEDICATED

TO MY

BELOVED PARENTS

ACKNOWLEDGEMENTS

December, 2015   **Md. Saiful Alam**

ABSTRACT

The nominal compositions of $Bi_{1-x}Gd_xMnO_3$ (x = 0.00-0.12) ceramics were synthesized by conventional solid state reaction technique and their morphological, dielectric and magnetic properties were investigated. The field emission scanning electron microscopy images and their respective histograms demonstrate that due to the substitution of Gd, the average grain size was reduced with a narrow size distribution. Particularly, for 12 % Gd substitution the average size was reduced up to around ~200 nm which is much smaller than that of undoped $BiMnO_3$ ceramic. The substitution of Gd also generated significant amount of oxygen vacancies and the oxygen vacancies were gradually increased with Gd doping concentration. Compared to the undoped $BiMnO_3$, the dielectric constant was stable in Gd doped $BiMnO_3$ ceramics over a wide range of high frequencies (10^4 to 10^8 kHz) by suppressing the dispersion at low frequencies. The substitution of Gd in place of Bi also reduced the dielectric constant, particularly at low frequencies. The reduction of dielectric constant at low frequencies in Gd doped $BiMnO_3$ ceramics may be associated with the large amount of oxygen vacancies which was generated upon the substitution of Gd. The magnetization versus magnetic field hysteresis loops were recorded using a Vibrating Sample Magnetometer (VSM) at room temperature. Due to the substitution of Gd, the magnetic parameters like remanent magnetization and coercive fields were enhanced nominally. The enhanced magnetic properties might be associated with the high magnetic moment of Gd^{3+} ion as well as the structural distortion in the perovskite with change in Mn–O–Mn bond angle. An asymmetric shift both in the field and magnetization axes of magnetization versus magnetic field curves was observed. This indicates the presence of exchange bias effect in these compounds notably at room temperature. Finally, the temperature dependent zero field cooled (ZFC) and field cooled (FC) magnetization curves demonstrate a ferromagnetic to paramagnetic transition around ~ 45 K in $BiMnO_3$. Below this phase transition temperature, there was a splitting between ZFC and FC curves which indicates the presence of a spin glass like state in undoped $BiMnO_3$. Due to the substitution of 4 % Gd in $BiMnO_3$, the ferromagnetic to paramagnetic transition was remain unchanged, however, the ZFC and FC curves were coincided with each other.

CONTENTS

CHAPTER 1
Introduction

CHAPTER 2
Theoretical Background

CHAPTER 3
Sample Preparation and Experimental Techniques

CHAPTER 4
Results and Discussion

CHAPTER 5
Conclusions

List of Figures

List of Table

Chapter 1

Introduction

1.1 Introduction

Multiferroic ceramics display a coexistence of two or more of the primary ferro-orders such as (anti)ferroelectricity, (anti)ferromagnetism, and/or ferroelasticity in the same phase [1-3]. The combination of ferro-orders in multiferroics often means that the different properties interact with each other and then this allows the possibility of switching magnetically ordered states using electric fields or electrically ordered states using magnetic fields. These materials have attracted considerable research interest due to their potential applications in information storage, emerging field of spintronics, switchable spin valves, high frequency filters and sensors [4-6]. As a potential candidate for practical applications among the limited choices offered by the multiferroic materials, $BiFeO_3$ with rhombohedrally distorted perovskite ABO_3 (A = Bi, B = Fe) structure has been investigated extensively due to its multiferroic properties at room temperature (RT) [4]. Particularly, in order to obtain better multiferroic properties with multifunctional activities the Bi ion of this material was doped by rare earth lanthanide ions such as La^{3+} [7], Gd^{3+} [8], Sm^{3+} [9] etc. or divalent ions like (Ca^{2+}, Sr^{2+}, Pb^{2+}, Ba^{2+}) [10, 11]. The partial substitution of Fe by ions such as Ti^{4+} [12, 13] or Cr^{3+} [14] was also found to improve the magnetism and ferroelectricity in $BiFeO_3$. Among the limited multiferroics, the simple perovskite $BiMnO_3$ has gained renewed and ever-increasing research interest since last few years [15-17]. However, there are only few literatures which reported results concerning the favourable effect of the substitution of rare earth lanthanide ions or divalent ions on the structural and functional properties of $BiMnO_3$. Notably, $BiMnO_3$ is a well established ferroelectric below 500 K and ferromagnet below 100 K [15]. Both the ferroelectric and ferromagmetic characteristics made this material potentially interesting for technological applications and in studying magnetoelectric interactions.

In this present investigation, the influence of the partial substitution of Bi by rare earth lanthanide ion Gd^{3+} in $BiMnO_3$ system was reported. It is intend to observe the substitutional effect on the morphological, dielectric and magnetic properties of

$Bi_{1-x}Gd_xMnO_3$ (x = 0.00-0.12) ceramics. Gd was chosen as a doping element as it is magnetically active (effective magnetic moment is 8 Bohr magneton) and the ferromagnetic transition temperature (Curie temperature) of Gd is close to room temperature [4]. Moreover, the ionic radius of Gd^{3+} (0.938 Å) ion is much smaller than that of Bi^{3+} (1.17 Å) ion which can lead large lattice distortion [18]. It is observed that due to the effect of Gd substitution, morphological and magnetic properties of these ceramics were improved. Also, an asymmetry exhibiting shifts both in the field and magnetization axes of M-H curves was observed due to the substitution of Gd in place of Bi in $BiMnO_3$ ceramics, which indicates the presence of exchange bias (EB) effect in these compounds at room temperature.

1.2 Aim and Objectives

The main objectives of the present research are as follows:

(a) Preparation of various nominal compositions of $Bi_{1-x}Gd_xMnO_3$ (x = 0.0, 0.04, 0.8, 0.12) ceramics using solid state reaction method.

(b) Investigation of the surface morphology of the samples using field emission scanning electron microscopy (FESEM).

(c) Investigation of the oxygen vacancies and phase purity in each composition using X-ray photoelectron spectroscopy (XPS) technique.

(d) Investigation of the dielectric properties of the ceramics as a function of frequencies at room temperature.

(e) Investigation of the magnetic properties such as remanent magnetization (M_r) and coercivity (H_c) of different compositions from magnetization versus applied magnetic field (M-H) hysteresis loops.

(f) Investigation of the phase transition temperature and temperature dependent magnetic properties using (SQUID) magnetometer.

1.3 Summary of the Thesis

The summary of the thesis are as follows:

Chapter 1 of this thesis deals with the introduction, importance and objectives of the present work.

Chapter 2 gives a brief overview of the materials, theoretical background.

Chapter 3 presents the details of the sample preparation and describes the descriptions of different measurements that have been used in this research work.

Chapter 4 is dedicated to the results of various investigations of the study and explanation of results in the light of existing theories.

The conclusions drawn from the overall experimental results are presented in **chapter 5.**

References:

[1] Eerenstein, W., Mathur, N. D., Scott, J. F., "Multiferroic and magnetoelectric materials", Nature 442, pp-759-765, 2006.

[2] Cheong, S. W., Mostovoy, M., "Multiferroics: a magnetic twist for ferroelectricity", Nature Materials 6, pp-13-20, 2007.

[3] Ramesh, R., "Materials science: Emerging routes to multiferroics", Nature 461, pp-1218-1219, 2009.

[4] Lazenka,V. V., Zhang, G., Vanacken, J., Makoed, I. I., Ravinski, A. F., Moshchalkov, V. V., "Structural transformation and magnetoelectric behaviour in $Bi_{1-x}Gd_xFeO_3$ multiferroics", J. Phys. D: Appl. Phys., 45, 125002, 2012.

[5] Tirupathi, and Chandra, A., "Stabilization of dielectric anomaly near the magnetic phase transition in Ca^{2+} doped $BiFeO_3$ multifunctional ceramics", J. of Alloys and Compounds, 564, pp-151-157, 2013.

[6] Xu, X., Guoqiang, T., Huijun, R., and Ao, X., "Structural, electric and multiferroic properties of Sm-doped $BiFeO_3$ thin film prepared by the sol–gel process", Ceramics International, 39, pp-6223-6228, 2013.

[7] Bras, G. L., Colson, D., Forget, A., Genand-Riondet, N., Tourbot, R., and Bonville, P., "Magnetization and magnetoelectric effect in $Bi_{1-x}La_xFeO_3$ (0≤x≤0.15)", Phys. Rev. B 80, 134417, 2009.

[8] Uniyal, P., Yadav, K.L., "Study of dielectric, magnetic and ferroelectric properties in $Bi_{1-x}Gd_xFeO_3$", Materials Letters, 62, pp-2858-2861, 2008.

[9] Khomchenko, V. A., Paixao, J. A., Costa, B. F. O., Karpinsky, D. V., Kholkin, A. L., Troyanchuk, I. O., Shvartsman, V. V., Kleeman, W., and Borisov, P., "Structural, ferroelectric and magnetic properties of $Bi_{0.85}Sm_{0.15}FeO_3$ perovskite", Crystal Research and Technology, 46, pp-238-242, 2011.

[10] Catalan, G., Sardar, K., Church, N. S., Scott, J. F., Harrison, R. J., and Redfern, S. A. T., "Effect of chemical pressure on the magnetic transition of multiferroic $Bi_{1-x}Ca_xFeO_3$", Phys. Rev. B 79, 212415, 2009.

[11] Khomchenko, A., Kiselev, D. A., Vieira, J. M., Jian, L., Kholkin, A. L., Lopes, A. M. L., Pogorelov, Y. G., Araujo, J. P., and Maglione, M., "Effect of diamagnetic Ca, Sr, Pb, and Ba substitution on the crystal structure and multiferroic properties of the $BiFeO_3$ perovskite ", J. Appl. Phys. 103, 024105, 2008.

[12] Basith, M. A., Kurni, O., Alam, M. S., Sinha, B. L., and Bashir Ahmmad., "Room temperature dielectric and magnetic properties of Gd and Ti co-doped $BiFeO_3$ ceramics", J. Appl. Phys. 103, 024105, 2014.

[13] Reetu., Agarwal, A., Sanghi, S., Ashima., and Neetu Ahlawat., "Improved dielectric and magnetic properties of Ti modified $BiCaFeO_3$ multiferroic ceramics", J. Appl. Phys. 113, pp-023908-023906, 2013.

[14] Cheng, L. B., Le, C. C., Zhi, X., Qian, X., "Effect of Cr substitution on the multiferroic properties of $BiFe_{1-x}Cr_xO_3$ compounds", Phys. Lett. A, 374, pp-4265-4268, 2010.

[15] Chou, C. C., Huang, C. L., Mukherjee, S., Chen, Q. Y., Sakurai, H., Belik, A. A., Takayama-Muromachi, E., and Yang, H. D., "Multiple magnetic transitions in multiferroic $BiMnO_3$", Phys. rev. B 80, 184426, 2009.

[16] Grizalez, M., Mendoza, G.A., and Prieto, P., "Analysis of multiferroic properties in $BiMnO_3$ thin films", Journal of Physics: Conference Series 167, 012035, 2009.

[17] Belik, A. A., and Muromachi, E. T., "Magnetic Properties of $BiMnO_3$ Studied with Dc and Ac Magnetization and Specific Heat", Inorg. Chem. 45, pp-10224-10229, 2006.

[18] Guo, R., Fang, L., Dong, W., Zheng, F., and Shen, M., "Enhanced Photocatalytic Activity and Ferromagnetism in Gd Doped $BiFeO_3$ Nanoparticles", J. Phys. Chem. C, 114, 21390, 2010.

Chapter 2

Theoretical Background

2.1 Multiferroics

Multiferroics have been formally defined as materials that exhibit more than one primary ferroic order parameter simultaneously. The four basic primary ferroic order parameters are ferromagnetism, ferroelectricity, ferroelasticity [1] and ferrotoroidicity [2]. The definition of schmid emphasizes "the same phase". In fact, the definition can be expanded to include non-primary order parameters, such as antiferromagnetism, ferrimagnetism and antiferroelectricity.
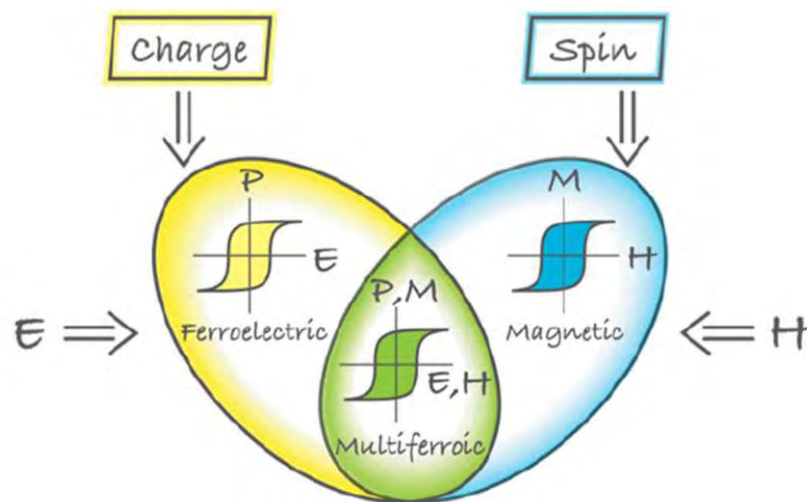
Figure 2.1: A schematic diagram of multiferroic

If the coupling between electric and magnetic order parameters exists, a multiferroic material becomes a magnetoelectric material. But a magnetoelectric (or a multiferroic) material does not necessary to be a multiferroic (or a magnetoelectric) material [3]. The history of magnetoelectric multiferroics can be traced back to the 1960s [4]. In the most general sense the field of multiferroics was born from studies of magnetoelectric systems. In recent 10 years, there is a great revival in multiferroics. In 2000, Nicola A. Hill gave an answer about scarcity of ferromagnetic ferroelectric coexistence [5]. In 2003 the large ferroelectric polarization was discovered in epitaxially grown thin films of $BiFeO_3$ [6]. The same year, the strong magnetic and electric coupling was found in orthorhombic $TbMnO_3$ [7] and $TbMn_2O_5$ [8]. The recent studies of multiferroics show the importance of collaboration between experiment technology and modeling design.

2.1.1 Classification of multiferroic

Multiferroic materials are generally two types; namely single phase and composite materials. Single-phase multiferroics are those materials that show both ferroelectric and ferromagnetic order [9-16]. Thus multiferroicity is intrinsic of the material. Khomskii classified single-phase multiferroics in two big groups and other subgroups [17], according to the physical mechanism behind ferroelectricity.

The scarcity of single phase multiferroic material makes composite materials an interesting alternative [16, 18-24]. In opposition to single-phase multiferroics, multiferroic order is not intrinsic but results from the combination of two materials that are ferroelectric and ferromagnetic, separately. Therefore, the availability of ferromagnetic and ferroelectric materials at room temperature makes easy to obtain multiferroic composite materials at room temperature.

Single-phase multiferroics can be classified into two types namely Type-I multiferroics and Type-II multiferroics. Type-I multiferroics are those materials in which ferroelectricity and magnetism have different sources; usually they show large polarization values and ferroelectricity appears at much higher temperatures than magnetism. This difference in transition temperatures reveals that both orders involve different energy scales and mechanisms, which provokes the occurrence of weak magnetoelectric coupling. $BiFeO_3$ is the example of type-1 multiferroic.

Type-II multiferroics correspond to materials in which magnetism causes ferroelectricity, implying a strong coupling between them. These show smaller electric polarization values and ferroelectricity always appears at lower temperature than magnetic order (always antiferromagnetic). $TbMnO_3$ is the example of type-II multiferroics.

2.1.2 Magnetoelectric effect

In multiferroic materials, the magnetoelectric effect (ME) is a very important phenomenon. The induction of electric polarization by means of a magnetic field and the induction of magnetization by means of a magnetic field are defined as the magnetoelectric effect. Mathematically

$$P_i(E,H) = -\frac{\partial F}{\partial E_i} = P_i^S + \varepsilon_0 \varepsilon_{ij} E_j + \alpha_{ij} H_j + \frac{1}{2} \beta_{ijk} H_j H_k + \gamma_{ijk} H_i E_j - ..... \qquad (2.1)$$

$$M_i(E,M) = -\frac{\partial F}{\partial H_i} = M_i^S + \mu_0 \mu_{ij} H_j + \alpha_{ij} E_i + \beta_{ijk} E_i H_j + \frac{1}{2} \gamma_{ijk} E_j E_k - ..... \qquad (2.2)$$

Where, ε is the permittivity, μ is the permeability, α is a second rank tensor known as the magnetoelectric susceptibility tensor, P_i is the electric polarization and M_i is the magnetization of the material (with the superscript S denoting spontaneous components).

2.2   General feature of magnetism

2.2.1 Origin of magnetism

Magnetism originates from the spin and orbital magnetic motions of an electron and it depends on how the electrons interact with one another. Different types of magnetism can introduce with the help of how materials respond to magnetic fields. Electricity is the movement of electrons, whether in a wire or in an atom, so each atom represents a tiny permanent magnet in its own right. The circulating electron produces its own orbital magnetic moment, measured in Bohr magnetons (μ_B), and there is also a spin magnetic moment associated with it due to the electron itself spinning, like the earth, on its own axis (illustrated in figure 2.2).
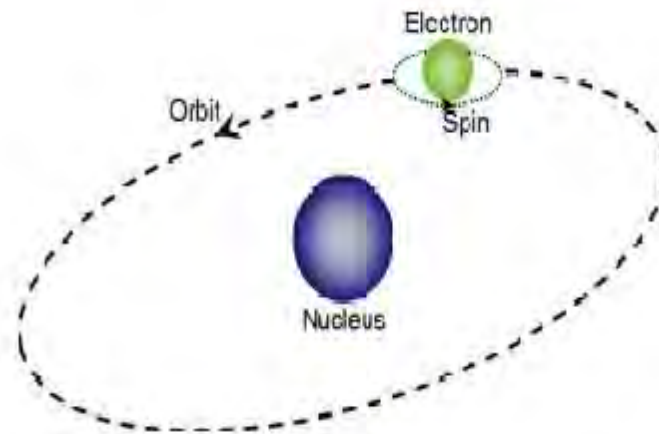
Figure 2.2: The orbit of a spinning electron about the nucleus of an atom.

In most materials there are resultant magnetic moments, due to the electrons being grouped in pairs causing the magnetic moment to be cancelled by its neighbor. In certain

magnetic materials the magnetic moments of a large proportion of the electrons align, producing a unified magnetic field. The field produced in the material (or by an electromagnet) has a direction of flow and any magnet will experience a force trying to align it with an externally applied field, just like a compass needle. The magnetic moment of a current carrying conductor is given by

$$\mu = IA \qquad \dots \qquad \dots \qquad \dots \qquad (2.3)$$

Where I is the current in Ampere and A is the area in m^2. The magnetic moment of an electron in orbit is given by

$$\mu = \pi r^2 (ev/2\pi r) = evr/2 \qquad \dots \qquad \dots \qquad (2.4)$$

Where r is the radius of orbit, e charge and v is the velocity of electron. The angular momentum of an electron must be an integral multiple of Planck's constant

$$mvr = nh/2\pi \qquad \dots \qquad \dots \qquad (2.5)$$

Where m is the mass and h is the Planck's constant. If the electron revolves in the first orbit then n = 1. Therefore orbital magnetic moment of an electron is given by from equation (2.4) and (2.5)

$$\mu = eh/4\pi m \qquad \dots \qquad \dots \qquad \dots \qquad (2.6)$$

Which is known as Bohr magneton, the smallest possible orbital magnetic moment. Similarly the smallest possible magnetic moment due to spin of the electron is

$$\mu = eh/4\pi m \qquad \dots \qquad \dots \qquad \dots \qquad (2.7)$$

According to quantum theory the spin of electrons has only two possibilities +1/2 or -1/2. Similar to equation (2.6), we can write in the form

$$\mu = (e/2m)S \quad \dots \qquad \dots \qquad \dots \qquad (2.8)$$

Where S is the spin quantum number here given by $(1/2).(h/2\pi)$. In short,

$$\mu = g.(e/2m).S \qquad \dots \qquad \dots \qquad \dots \qquad (2.9)$$

Here g is the term known as g-factor. When $g = 2$, the spin contribution arises and when $g = 1$ the orbital contribution arises. The mass of the nucleus is so large that the magnetic moment contribution can be neglected compared to the electronic magnetic moment. The gyromagnetic ratio is proportional to the g-factor and 'g' arises due to the precession of the electrons similar to the precession of a top in a gravitational force. The value of g tells us whether the origin of magnetic moment is spin or orbital motion of electrons.

The origin of magnetic moments in solids as a consequence of overlapping of the electronic wave functions with those of neighboring atoms. This condition is best fulfilled by some transition metals and rare-earths elements. The exchange interactions depend sensitively upon the inter-atomic distance and the nature of the chemical bonds, particularly of nearest neighbor atoms. Thus the nature of magnetization produced depends on the number of unpaired valence electrons present in the atoms of the solid and on the relative orientation of the neighboring magnetic moments. The main distinction is that in some materials there is no collective interaction of atomic magnetic moments, whereas in other materials there is a very strong interaction between atomic moments.

2.2.2 Magnetic moment of atoms and electrons

The electron is a charged particle, so its angular momentum comes from two types of motion, spin and orbital motion. From classical electrodynamics, a rotating electrically charged body creates a magnetic dipole with magnetic poles of equal magnitude but opposite polarity. This analogy holds as an electron indeed behaves like a tiny bar magnet. One consequence is that an external magnetic field exerts a torque on the electron magnetic moment depending on its orientation with respect to the field.

The magnetic energy of an electron is approximately twice what it should be in classical mechanics. The factor of two multiplying the electron spin angular momentum comes from the fact that it is twice as effective in producing magnetic moment. This factor is called the electronic spin g-factor. The persistent early spectroscopists, such as Alfred Lande, worked out a way to calculate the effective of the various directions of angular momenta. The resulting geometric factor is called the Lande g-factor. The intrinsic magnetic moment of a particle with charge q, mass m and spin s, is

$$\mu_m = g \frac{q}{2m} s \qquad \ldots \qquad \ldots \qquad \ldots \qquad (2.10)$$

Where the dimensionless quantity „g" is called the g-factor. The g-factor is an essential value related to the magnetic moment of the subatomic particles and corrects for the precession of the angular momentum. The value of g is 2.002319, which arises from the Dirac equation, a fundamental equation connecting the electron spin with its electromagnetic properties. The total spin magnetic moment of the electron is

$$\mu_s = -g_s \mu_B (s/\hbar) \quad \ldots \quad \ldots \quad \ldots \quad (2.11)$$

Where $g_s = 2$ in Dirac mechanics, but is slightly larger due to Quantum Electrodynamics effects, μ_B is the Bohr magneton and s is the electron spin. The z component of the electron magnetic moment is

$$\mu_z = -g_s \mu_B m_s \quad \ldots \quad \ldots \quad \ldots \quad (2.12)$$

Where, m_s is the spin quantum number.

If the electron is visualized as a classical charged particle literally rotating about an axis rounds an atomic nucleus with a radius r, angular momentum L and an angular velocity ω leads to the formula

$$L = mr^2 \omega \quad \ldots \quad \ldots \quad \ldots \quad (2.13)$$

The magnetic moment μ_L of the electron can be defined as the product of a circular electrical current I around a closed area A

$$\mu_L = I.dA \quad \ldots \quad \ldots \quad \ldots \quad (2.14)$$
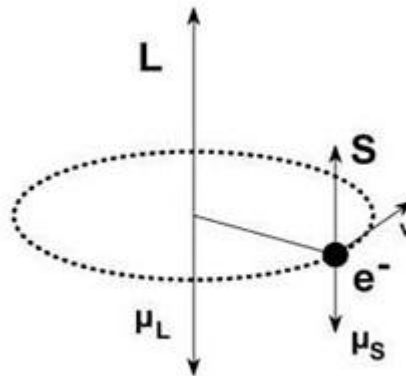
Figure 2.3: Angular momentum L, spin S and corresponding magnetic moments for an electron revolving around the atomic nucleus.

By construction of I for the revolving charge e, by the above we get for the total magnetic dipole moment

$$\mu_L = -\frac{eL}{2m_e} = -\mu_B \sqrt{l(l+1)} \quad \ldots \quad \ldots \quad (2.15)$$

Where, μ_B is the Bohr magneton. The z component of the orbital magnetic dipole moment for an electron with a magnetic quantum number m_l is given by

$$\mu_z = -\mu_B m_l \quad \ldots \quad \ldots \quad \ldots \quad (2.16)$$

2.2.3 Magnetic behavior

The origin of magnetism lies in the orbital and spin motions of electrons and how the electrons interact with one another. The best way to introduce the different types of magnetism is to describe how materials respond to magnetic fields. This may be surprising to some, but all matter is magnetic. It's just that some materials are much more magnetic than others. The main distinction is that in some materials there is no collective interaction of atomic magnetic moments, whereas in other materials there is a very strong interaction between atomic moments. Since the response of a material to a magnetic field (H) is characteristic of the magnetic induction of flux density (B) and the effect that a material has upon the magnetic induction in a magnetic field is represented by the magnetization (M). Thus a universal equation can be established by relating these three magnetic quantities as

$$B = \mu_0 (H + M) \qquad \ldots \qquad \ldots \qquad (2.17)$$

$$B = \mu H \qquad \ldots \qquad \ldots \qquad (2.18)$$

Where μ_0 is permeability of a vacuum, a universal constant, which has a value of $4\pi \times 10^{-7} H/m$ and μ is the permeability of a material. In equation (2.17) one can see that $\mu_0 H$ is the magnetic induction generated by the field alone and $\mu_0 M$ is the additional magnetic induction contributed by a material. The magnetic susceptibility χ is defined as the ratio if magnetization to magnetic field and it is a dimensionless quantity that determines how easily a specimen can be magnetized.

$$\chi = \frac{M}{H} \qquad \ldots \qquad \ldots \qquad (2.19)$$

The magnetic susceptibility and the permeability are related as follows

$$\mu = \mu_0 (1 + \chi) \qquad \ldots \qquad \ldots \qquad (2.20)$$

The magnetic behavior of materials can be classified into the following five major groups

  i. Diamagnetism

  ii. Paramagnetism

  iii. Ferromagnetism

  iv. Ferrimagnetism

  v. Antiferromagnetism

Different materials respond to applied magnetic fields in different ways. Materials in the first two groups are those that exhibit no collective magnetic interactions and are not magnetically ordered. Materials in the last three groups exhibit long-range magnetic order below a certain critical temperature. Ferromagnetic and ferromagnetic materials are usually what we consider as being magnetic (i.e., behaving like iron). The remaining three are so weakly magnetic that they are usually thought of as "nonmagnetic". Different magnetic behavior describes how adjacent magnetic moments would interact with each other at absolute zero. The interactions are shown in Figure 2.4 and described below:

i. Diamagnetism

The substances whose atoms have zero resultant magnetic moment are called as diamagnetic substances. The behavior of diamagnetic substances in external magnetic field is known as diamagnetism, a fundamental property of all matter. In the absence of external magnetic field atoms of diamagnetic substances have zero resultant magnetic moment. If the diamagnetic substance is placed in external magnetic field then magnetic lines of induction will pass through electronic orbits. This will produce induced current. The induced current produces induced magnetic moment in opposite direction to that of the applied field. Hence atomic magnets of diamagnetic substances will align in opposite direction to that of the direction of external magnetic field. The resultant magnetic moment of the substance increases and it will show weak magnetic property. The diamagnetic substances are slightly repelled by the magnet. In diamagnetic materials the magnetic susceptibility is negative. Usually its magnitude is of the order of -10^{-6} to -10^{-5}. Diamagnetic materials have a relative magnetic permeability that is less than 1. In diamagnetic materials the susceptibility nearly has a constant value independent of temperature. Most of the materials are diamagnetic e.g. Mercury, air, water, alcohol, gold, bismuth, copper, hydrogen, zinc, diamond, NaCl, nitrogen, magnesium, silver etc.

ii. Paramagnetism

The substances whose atoms have resultant magnetic dipole moment slightly greater than zero are called as paramagnetic substances. The behaviour of paramagnetic substances in external magnetic field is known as paramagnetism. In the absence of external magnetic field atomic magnets of paramagnetic substances will point out in all

possible directions. Hence the resultant magnetic moment of the substance will be less and it will not show magnetic property. If the paramagnetic substance is placed in a magnetic field then atomic magnets of paramagnetic substances will align in the same direction as that of the direction of external magnetic field. Hence resultant magnetic moment of the substance increases and it will show magnetic property. Paramagnetic materials attract and repel like normal magnets when subject to a magnetic field. Under relatively low magnetic field saturation when the majority of the atomic dipoles are not aligned with the field, paramagnetic materials exhibit magnetization. In paramagnetic material alignment of the atomic dipoles with the magnetic field tends to strengthen it, and is described by a relative magnetic permeability, μ_r greater than unity (or, equivalently, a small positive magnetic susceptibility greater than zero). The susceptibility is however is also very small with the order of 10^{-4} to 10^{-5}. A few examples of paramagnetic materials are oxygen, glass, paper, aluminium, platinum, chromium, sodium, manganese, copper chloride etc. The susceptibility of a paramagnetic material is inversely dependent on temperature and related with Curie law [25]

$$\chi = \frac{C}{T} \qquad \ldots \qquad \ldots \qquad \ldots \qquad (2.21)$$

Where C is the Curie constant.
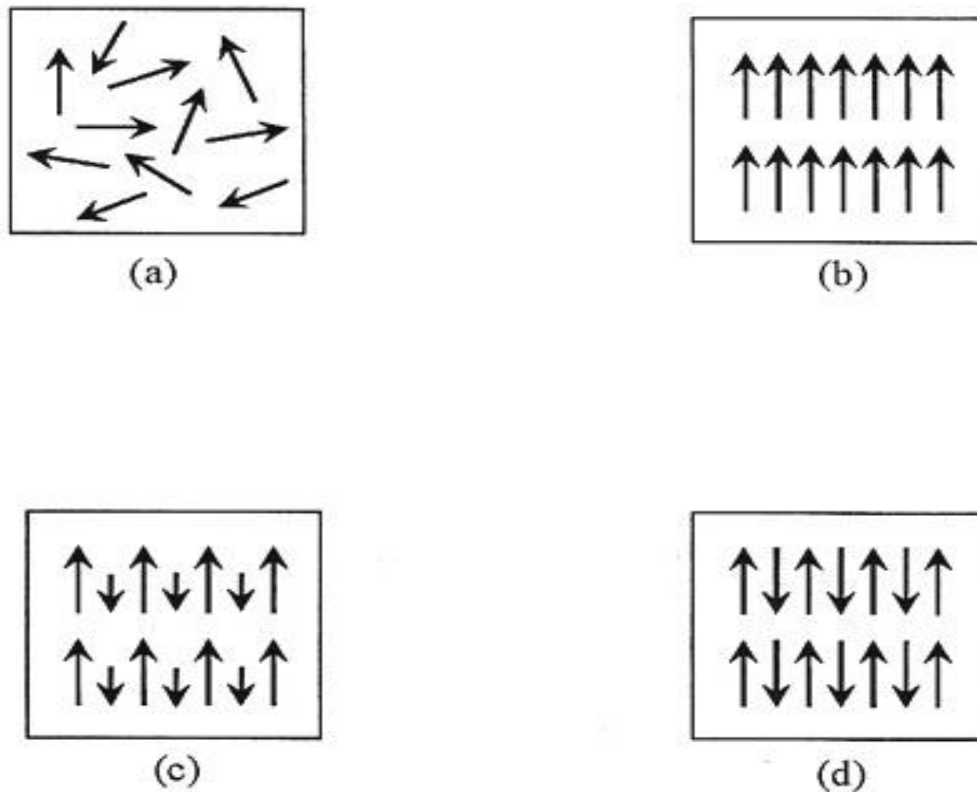
Figure 2.4: Varieties of magnetic orderings (a) paramagnetic, (b) ferromagnetic, (c) ferromagnetic and (d) antiferromagnetic.

iii. Ferromagnetism

The substances whose atoms have resultant magnetic dipole moment greater than diamagnetic and paramagnetic substances are called as ferromagnetic substances. The behavior of ferromagnetic substances in external magnetic field is known as ferromagnetism. In the absence of external magnetic field atomic magnets of ferromagnetic substance interact with each other and forms the groups called as domains.

In the absence of external magnetic field, domains of the ferromagnetic substances will point out in all possible direction. Hence resultant magnetic moment of the substance will be less and it will not show magnetic property. If the ferromagnetic substance is placed in a weak magnetic field then, some domains will point out in same direction as that of external magnetic field. Hence the resultant magnetic moment of the substance increases and it will show magnetic property. If external magnetic field is removed from the substance then domains of substances will point out in all possible direction. Hence

the resultant magnetic moment of the substance decreases to its original value and it loses magnetic property. If the ferromagnetic substance is placed in a strong magnetic field then, all domains of substance will align in the same direction as that of the direction of external magnetic field. In this case, domains will grow in their size also. Hence resultant magnetic moment of substance increases largely and it will show strong magnetic property. If the external magnetic field is removed from the substance then domains of the substance will remain in the same direction. Hence resultant magnetic moment of the substance remains to its maximum value. .Therefore, it will not lose magnetic property. The permeability of ferromagnetic substance is much greater than 1. The elements Iron, cobalt, nickel and many of their alloys are ferromagnetic materials.

As the temperature increases, thermal oscillation, or entropy, competes with the ferromagnetic tendency for spins to align. When the temperature rises beyond a certain point, called the Curie temperature, there is a second-order phase transition and the system can no longer maintain a spontaneous magnetization, although it still responds paramagnetically to an external field [26]. Below that temperature, there is a spontaneous symmetry breaking and random domains form (in the absence of an external field). The Curie temperature itself is a critical point, where the magnetic susceptibility is theoretically infinite but it''s real value is 1 to 10^6 and, although there is no net magnetization. The susceptibility of ferromagnetic material does not follow the Curie law, but displayed a modified behavior defined by Curie-Weiss law [27]

$$\chi = \frac{C}{T - \theta} \qquad \ldots \qquad \ldots \qquad \ldots \qquad (2.22)$$

Where C is a constant and θ is called Weiss constant. For ferromagnetic materials, the Weiss constant is almost identical to the Curie temperature (T_c).

There are two distinct characteristics of ferromagnetic materials, spontaneous magnetization and the existence of magnetic ordering temperature. The spontaneous magnetization is the net magnetization that exists inside a uniformly magnetized microscopic volume in the absence of a field. The magnitude of this magnetization, at 0 K, is dependent on the spin magnetic moments of electrons. The saturation magnetization is the maximum induced magnetic moment that can be obtained in a magnetic field (H_{sat}); beyond this field no further increase in magnetization occurs.

Saturation magnetization is an intrinsic property, independent of particle size but dependent on temperature.

iv. Antiferromagnetism

Antiferromagnetism exhibits in the material whose spins of magnetic electrons align in a regular pattern with neighboring spins pointing in opposite directions. This is the opposite of ferromagnetism. Generally, antiferromagnetic materials exhibit antiferromagnetism at a low temperature, and become disordered above a certain temperature; the transition temperature is called the Néel temperature. Above the Néel temperature, the material is typically paramagnetic [28].

The antiferromagnetic behaviour at low temperature usually results in diamagnetic properties, but can sometimes display ferrimagnetic behaviour, which in many physically observable properties are more similar to ferromagnetic interactions. However, in antiferromagnetic materials, the conditions are such that it is energetically favorable for the spins to oppose, leading to no overall magnetization.

The magnetic susceptibility, χ of an antiferromagnetic material will appear to go through a maximum as the temperature is lowered; in contrast, that of a paramagnet will continually increase with decreasing temperature. Antiferromagnetic materials have a negative coupling between adjacent moments and low frustration. Antiferromagnetic materials are relatively uncommon. Common examples of materials with antiferromagnetic ordering include MnO, FeO, CoO and NiO.

v. Ferrimagnetism

Ferrimagnetism is a special case of antiferromagnetism, where the material consists of a lattice of rigidly alternating spins of different magnitudes. As in antiferromagnetism, the adjacent magnetic spins align antiparellel, figure 2.4 the ferromagnetic spin allignment. However, since the adjacent spins are of different magnitudes, the resulting material exhibits a net magnetic moment in the absence of an applied magnetic field. The behavior of susceptibility of a ferrimagnetic material also obeys Curie-Weiss law and has a relative permeability greater than 1.

In ionic compounds, such as oxides, more complex forms of magnetic ordering can occur as a result of the crystal structure. In ferromagnetic material the magnetic structure is composed of two magnetic sublattices (called A and B) separated by

oxygens. The exchange interactions are mediated by the oxygen anions. When this happens, the interactions are called indirect or superexchange interactions. The strongest superexchange interactions result in an antiparallel alignment of spins between the A and B sublattice. In ferrimagnets, the magnetic moments of the A and B sublattices are not equal and result in a net magnetic moment. Ferrimagnetism is therefore similar to ferromagnetism. It exhibits all the hallmarks of ferromagnetic behavior spontaneous magnetization, Curie temperatures, hysteresis, and remanence. However, ferro- and ferrimagnets have very different magnetic ordering.
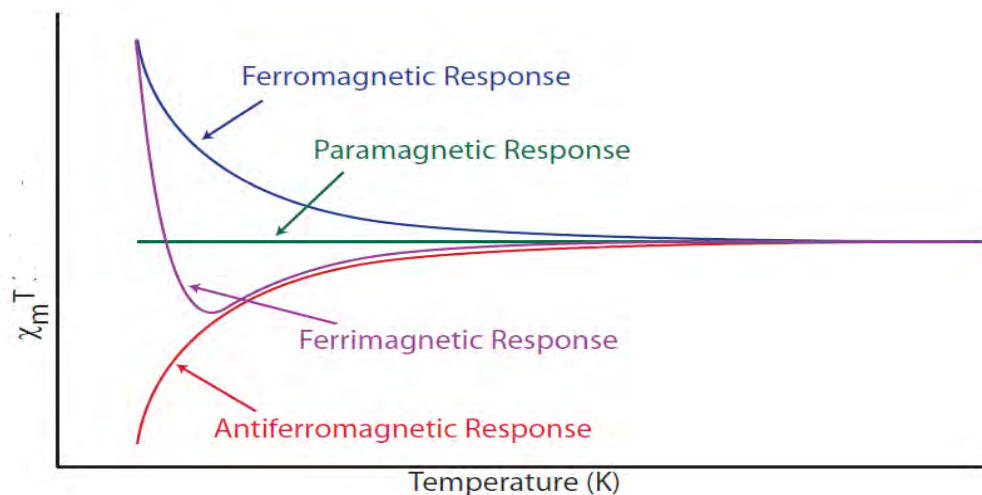
Figure 2.5: A typical plot for the susceptibility temperature product as a function of temperature is shown for paramagnetic, ferromagnetic, antiferromagnetic and ferrimagnetic materials.

2.3 Magnetization

Magnetization is the vector field that expresses the density of permanent or induced magnetic dipole moments in a magnetic material. The origin of the magnetic moments responsible for magnetization can be either microscopic electric currents resulting from the motion of electrons in atoms, or the spin of the electrons or the nuclei. Net magnetization results from the response of a material to an external magnetic field, together with any unbalanced magnetic dipole moments that may be inherent in the material itself; for example, in ferromagnets. Magnetization is not always homogeneous within a body, but rather varies between different points. Magnetization also describes how a material responds to an applied magnetic field as well as the way the material changes the magnetic field, and can be used to calculate the forces that result from those

interactions. It can be compared to electric polarization, which is the measure of the corresponding response of a material to an electric field in electrostatics. Physicists and engineers define magnetzation as the quantity of magnetic moment per unit volume. It is represented by a vector $\overline{M}$. Mathematically, magnetization can be defined according to the following equation:

$$\overline{M} = (N/V)\overline{m} = n\,\overline{m} \qquad \ldots \qquad \ldots \qquad \ldots \qquad (2.23)$$

Here, $\overline{M}$ represents magnetization; m is the vector that defines the magnetic moment; V represents volume and N is the number of magnetic moments in the sample. The quantity N/V is usually written as n, the number density of magnetic moments.

2.4 Hysteresis Loop

One of the most distinctive features of materials with bulk magnetism is hysteresis. Hysteresis is observed for ferromagnetic and ferromagnetic materials below their critical point and arises from rearrangement of domain walls within the material. In addition to the Curie temperature or critical point and saturation magnetization, ferromagnets can retain a memory of an applied field once it is removed. This behavior is called hysteresis and a plot of the variation of magnetization with magnetic field is called a hysteresis loop.

Magnetization M (or flux density B) and field intensity H are not proportional for ferromagnets and ferrimagnets. If the material is initially unmagnetized, then M or B varies as a function of H as shown in Figure-2.6. The curve begins at the origin, and as H is increased, the magnetization M or B field begins to increase slowly, then more rapidly, finally leveling off and becoming independent of H. This maximum value of B is the saturation flux density B_s and the corresponding magnetization is the saturation magnetization M_s. As the external field is applied, the domains that are oriented in directions favorable to (or nearly aligned with) the applied field grow at the expense of those that are unfavorably oriented. This process continues with increasing field strength until the macroscopic specimen becomes a single domain, which is nearly aligned with the field. Saturation is achieved when this domain, by means of rotation, becomes oriented with the *H* field. From saturation, point *S* in Figure 2.6, as the *H* field is reduced by reversal of field direction, the curve does not retrace its original path. A hysteresis effect is produced in which the *B* field lags behind the applied *H* field, or decreases at a

lower rate. At zero *H* field (point *R* on the curve), there exists a residual *B* field that is called the remanence, or remanent flux density, B_r; the material remains magnetized in the absence of an external *H* field.

Hysteresis behavior and permanent magnetization may be explained by the motion of domain walls. Upon reversal of the field direction from saturation (point *S* in Figure 2.6), the process by which the domain structure changes is reversed. First, there is a rotation of the single domain with the reversed field. Next, domains having magnetic moments aligned with the new field form and grow at the expense of the former domains. Critical to this explanation is the resistance to movement of domain walls that occurs in response to the increase of the magnetic field in the opposite direction; this accounts for the lag of *B* with *H*, or the hysteresis. When the applied field reaches zero, there is still some net volume fraction of domains oriented in the former direction, which explains the existence of the remanence B_r.

To reduce the *B* field within the specimen to zero (point *C* on Figure-2.6), an *H* field of magnitude H_c must be applied in a direction opposite to that of the original field; H_c is called the coercivity, or sometimes the coercive force. Upon continuation of the applied field in this reverse direction, as indicated in the figure; saturation is ultimately achieved in the opposite sense, corresponding to point S'. A second reversal of the field to the point of the initial saturation (point *S*) completes the symmetrical hysteresis loop and also yields both a negative remanence $(-B_r)$ and a positive coercivity $(+H_c)$.
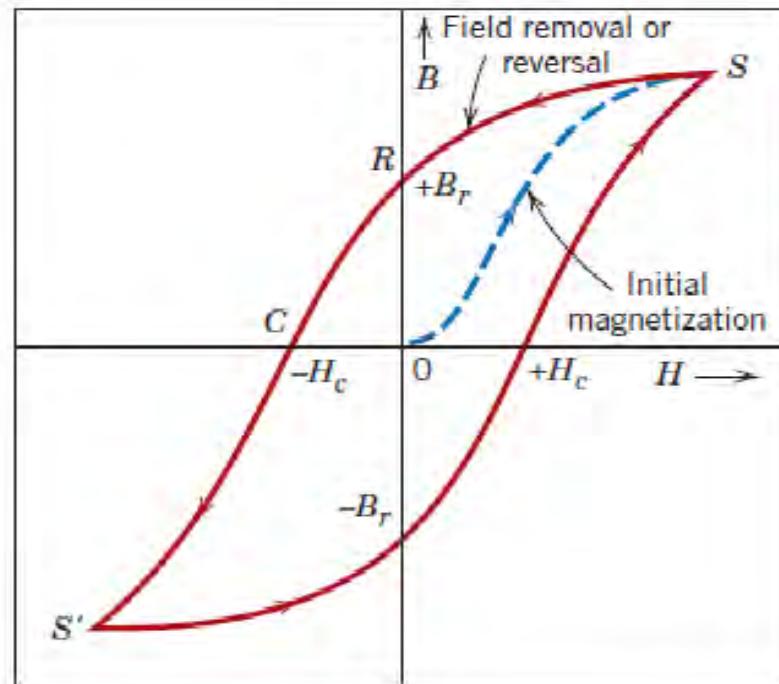
Figure 2.6: Magnetic flux density versus the magnetic field strength for a ferromagnetic material that is subjected to forward and reverse saturations (points S and S'). The hysteresis loop is represented by the solid red curve; the dashed blue curve indicates the initial magnetization. The remanence B_r and the coercive force H_c are also shown.

Coercive fields from 0.01 G to 15,000 G have been observed for different materials. In general materials with low coercive fields (< 1 G) have been termed "soft" magnets, while materials with high coercive field (>500 G) have been termed "hard" magnets.

2.5 Microstructure

A polycrystal is much more than many tiny crystals bounded together. The interfaces between the crystals, or the grain boundaries which separate and bound the grains, are complex and interactive interfaces. The whole set of a given materials properties (mechanical, chemical and especially electrical and magnetic) depend strongly on the nature of the microstructure.

In the simplest case, the grain boundary is the region, which accommodates the difference in crystallographic orientation between the neighbouring grains. For certain simple arrangements, the grain boundary is made of an array of dislocations whose number and spacing depends on the angular deviation between the grains. The ionic nature of ferrites leads to dislocation patterns considerably more complex than in metals,

since electrostatic energy accounts for a significant fraction of the total boundary energy [30]. For low loss ferrite, Ghate [29] states that the grain boundaries influence properties by

> 1) creating a high resistivity intergranular layer,
> 2) acting as a sink for impurities which may act as a sintering aid and grain growth modifiers.
> 3) providing a path for oxygen diffusion, this may modify the oxidation state of cations near the boundaries.

Besides the grain boundaries, ceramic imperfections can impede domain wall motion and thus reduce the magnetic property. The pores, cracks, inclusions, second phases as well as residual strain are also effects on magnetic property. Stresses are microstructural imperfections that can result from impurities or processing problems such as too rapid a cool. They affect the domain dynamics and are responsible for a much greater share of the degradation of properties than would expect [29].

Grain growth kinetics depends strongly on the impurity content. A minor dopant can drastically change the nature and concentration of defects in the matrix, affecting grain boundary motion, pore mobility and pore removal [30, 31]. The effect of a given dopant depends on its valence and solubility with respect to host material. If it is not soluble at the sintering temperature, the dopant becomes a second phase which usually segregates to the grain boundary.
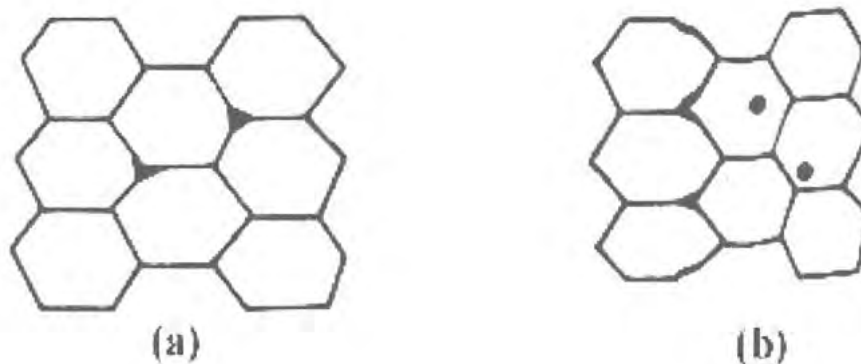
Figure 2.7: Porosity character: (a) intergranular and (b) intragranular.

The porosity of ceramic samples results from two sources, intragranular porosity and intergranular porosity, Figure-2.7. An undesirable effect in ceramic samples is the

formation of exaggerated or discontinuous grain growth which is characterized by the excessive growth of some grains at the expense of small, neighbouring ones, Figure-2.8. When this occurs, the large grain has a high defect concentration. Discontinuous growth is believed to result from one or several of the following: powder mixtures with high impurities; in ferrites containing Zn and/or Mn, a low O_2 partial pressure in the sintering atmosphere. When a very large grain is surrounded by smaller ones, it is called „duplex" microstructure.
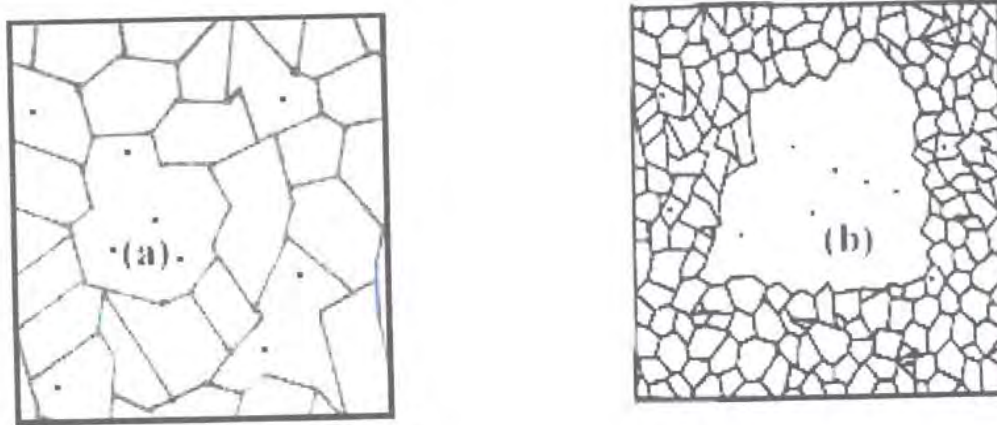
Figure 2.8: Grain growth (a) discontinuous and (b) duplex (schematic).

2.6 Spin Glass

During the last decade the term „spin glass" has become prominent in the literature on magnetism. It refers to magnetic alloys where the spins on the impurities become locked or frozen into random orientations below a characteristic temperature T_0. Interest in spin glasses was mainly stimulated by some AC susceptibility measurements which showed sharp, cusp-like peaks, accurately defining T_0 and suggesting that some type of phase transition was occurring. Spin class behaviors was first observed in fairly concentrated alloys (about 1 to 10 percent of impurities) of iron in gold (AuFe) and manganese in copper (CuMn). The first above two metals, as Au in the alloy (AuFe) is the host, and the second, as Fe, the impurity.

Among many types of the magnetic-ordered materials [32] a special place belongs to so-called spin glasses. Orientation of the elementary magnetic moments of spin glass atoms or clusters in temperatures below some value T_f has no spatial periodicity. It randomly varies in space, just like in the case of atoms that are casually located in usual glass. Unlike paramagnetics, where elementary magnetic moments fluctuate in time, spin

glasses are characterized below certain temperature by the presence of "frozen" magnetic moments. That is, the atom magnetic moments have nonzero average vector values in terms of time [33, 34]. The latter is confirmed by Mössbauer measurements, which demonstrate the presence of effective magnetic fields that influence magnetic atoms. As investigations show, the universal reason of occurrence of the spin glass condition is a combination of nuclear disorder and a competition of exchange interactions. Hence, study of a spin glass condition is part of the general problem of studying of atomic-disorder magnetics, that is, substances, in which the nuclear disorder is a consequence of random atomic distribution of various types (the chemical disorder) or a disordered distribution in atomic space of one type (vitreous or an amorphous condition). An ideal spatial order is observed in a perfect crystal. It represents a set of a big number of identical atoms or molecules, packed in a regular way in the volume of a crystal. The elementary type of the disorder is realized in a substitutional solid solution. In an ideal crystal it is possible to replace an atom of an element A with an atom of other element B without essential lattice distortion. If in this case, lattice points, where the replacement of atoms A with atoms B occurs, do not form a regular lattice, we have an example of a disorder of replacement. Otherwise, a so-called superlattice is created. Another type of a disordered system is materials, in which the atoms distribution does not correspond with the lattice. Amorphous materials and liquids are examples of this type.

2.7 Dielectrics

A dielectric material (dielectric for short) is an electrical insulator that can be polarized by an applied electric field as shown in figure 2.9. The word dielectric is derived from the prefix dia, originally from Greek, which means „through‟ or „across‟, thus the dielectric is referred to as a material that permits the passage of the electric flux but not particles. When a dielectric is placed in an electric field, electric charges do not flow through the materials as in a conductor, but only slightly shift from their average equilibrium positions causing dielectric polarization. Because of dielectric polarization, positive charges are displaced towards the field and negative charges shift in the opposite direction. This creates an internal electric field which reduces the overall field within the dielectric itself.
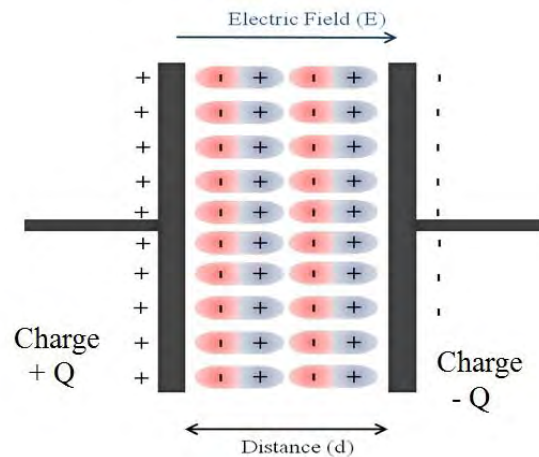
Figure 2.9: Schematic diagram of parallel electrodes separated by a dielectric material

The insulator material is called dielectric [35], is a material that resists the flow of electric charge. The valence electrons are tightly bonded to their atoms in insulating materials. These materials are used in electrical conductors without allowing current through themselves. The study of dielectric properties is concerned with the storage and dissipation of electric and magnetic energy in materials. So in dielectric, it is very important to explain various phenomena in electrics, optics and solid state physics.

There are two types of dielectric; they are polar dielectrics and non-polar dielectrics. In polar dielectric, a shift has occurred in the atomic structures such that the positive and negative charges have an asymmetrical alignment producing an electrical dipole but in non-polar dielectric this situation is absent.

2.7.1 Polarization

When the atoms or molecules of a dielectric are placed in an external electric field, the nuclei are pushed with the field resulting in an increased positive charge on one side while the electron clouds are pulled against it resulting in an increased negative charge on the other side. This process is known as polarization and a dielectric material in such a state is said to be polarized [35]. There are two principal methods by which a dielectric can be polarized, stretching and rotation.

2.7.2 Process of Polarization

The formation of an electric dipole or polarization can happen in a number of process or mechanisms [35]. At different frequency regimes each one contributes to dielectric response and their involvement are in different polarizable species. The basic

mechanism or processes are

1)   Electronic polarization
2)   Ionic or atomic polarization
3)   Orientation polarization
4)   Space charge polarization

2.7.2.1 Electronic Polarization

Electronic polarization occurs in all dielectric materials. Upon an external electric field being applied a slight relative shift of positive and negative electric charge in opposite directions occurs within an insulator, or dielectric. Polarization occurs when the induced electric field distorts the negative cloud of electrons around positive atomic nuclei in a direction opposite the field. This slight separation of charge makes one side of the atom somewhat positive and the opposite side somewhat negative. As soon as the electric field is removed the electrons and nuclei return to their original position and the polarization disappears.
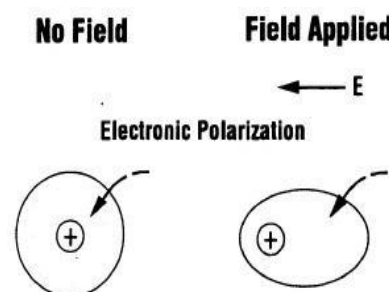
Figure 2.10: Electronic polarization

2.7.2.2 Atomic polarization

It is also known as ionic polarization. It involves the displacement of positive and negative ions in relation to one another within crystal structure when an electric field is applied. The magnitude of the dipole moment for each ion pair p_i is equal to the product of the relative displacement d_i and the charge on each ion as

$$p_i = qd_i \qquad \ldots \qquad \ldots \qquad \ldots \qquad (2.24)$$

Various popular effects like piezoelectricity, pyroelectricity, ferroelectricityetc occurs by ionic polarization phenomena. Wide range of polarization effects are possible through this mechanism depending upon the crystal structure, solid solution and various other factors.

Ionic polarization is inversely proportional to the mass of the ions and square of the

natural frequency of vibration of the ions. Covalently bonded ceramics do not show ionic polarization due to lack of charged atoms, but ionic bonded structures show ionic polarization. The frequency with which ions are displaced is of the same order as the lattice vibration frequency $\sim 10^{13}$ Hz. It is observed in ionic crystals and occurs up to the infrared region 10^{10}- 10^{13} Hz.
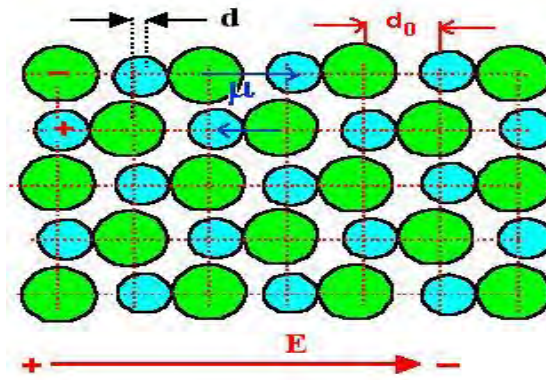
Figure 2.11: Atomic polarization

2.7.2.3 Dipolar polarization

This mode of polarization mainly attributed to the unequal charge distribution between partners in a molecule or complex ion. When a field is applied, these tend to line up with the electric dipoles in the direction of the field, giving rise to an orientation polarization. That is why this polarization is found only where substance possesses permanent dipole moments. Upon electric field these permanent moments rotate into the direction of the applied field, therefore contribute to the dipolar polarization. The tendency to alignment is counterbalanced by thermal vibrations of the atoms such that the polarization decreases with the increasing temperature.

Dipolar polarization occurs at lower frequencies of the field and thus can greatly affect the capacitive and insulating properties of glasses and ceramics in low frequency applications. Dipolar polarization is known as orientational polarization and it is both frequency and temperature dependent.
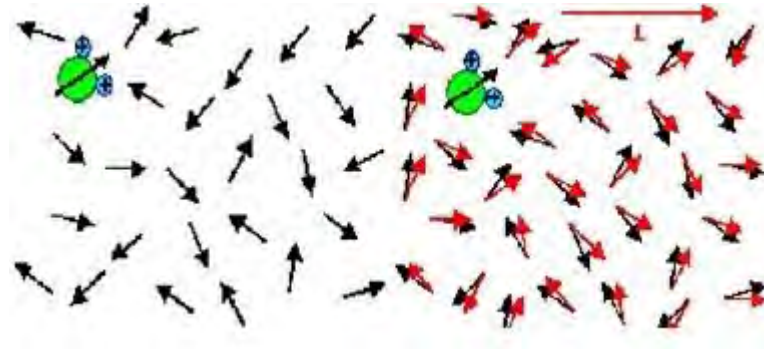
Figure 2.12: Dipolar polarization

2.7.2.4 Space charge polarization

The final source of polarization is mobile charges which are present because they are impeded by interfaces, because they are mot supplied at an electrode or discharged at an electrode. Or they are trapped in the material during fabrication process. Space charges resulting from these phenomena appear as an increase in capacitance as far as the exterior circuit is concerned. Space charge polarization occurs at low frequencies (50-60 Hz). A type of polarization is known as Maxwell-Wagner polarization is related to the space charge polarization because this type of polarization is occurred within the frequency range (10-10^4 Hz).
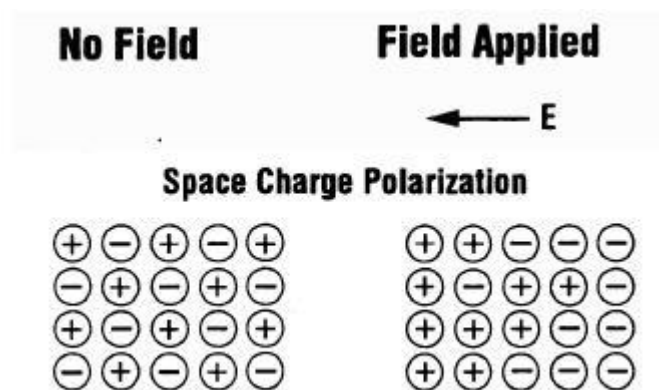
Figure 2.13: Space Charge polarization

The dielectric response of solids is a complex function of frequency, temperature, and type of solid. Under dc conditions all mechanism operates and the maximum polarization results which eventuates to the maximum of dielectric constants. An ideal dielectric is supposed to adjust itself instantaneously to any change in voltage. However in practice there is inertia to charge movement that shows up as a relaxation time for

charge transport. When the frequency of the applied field increases the mechanisms start to fade out and the value of polarizability starts.
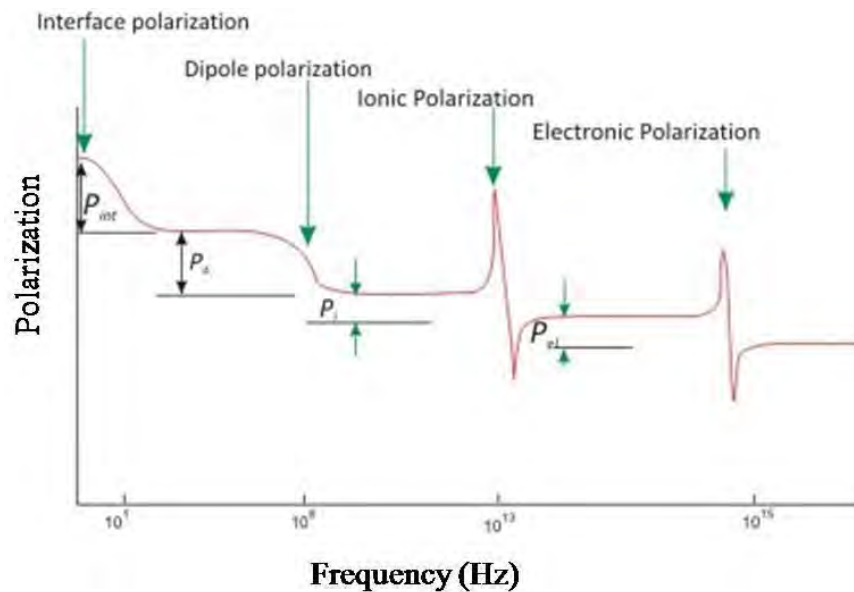
Figure 2.14: Variation of polarization with frequency

It is already been noticed that the electronic polarization is the only process that can follow the rapid change in the alternate field so to cause a variation in the polarizability. That is why this is still operative in the visible range of the spectrum.

Ionic polarization processes are able to follow an applied high frequency field and contribute to the dielectric constant at frequencies up to infrared region of the spectrum. Dipolar and space charge polarization have relaxation time corresponding to the particular system and process but in general participate and contribute only at lower frequencies.

2.7.3 Dielectric properties

Ceramics are mostly covalently bonded material hence electrically non-conductive or insulator. Importance of particular property depends on the application demand. For instance dielectric strength is an important parameter for application of ceramic as insulators used in power transmission line, load bearing general insulators, in house hold appliances, etc. In this kind of applications where frequency does not exceed 1 kHz, the breakdown strength, measure in kV/cm, together with mechanical strength are prime important factors. The dielectric constant (k) or loss factor ($\tan \delta$) does not matter

much. On the other hand, for capacitor and electronics applications just the opposite required the values of k and $\tan\delta$ are of prime importance, not only their room temperature values but also as function of temperature and frequency. These are intrinsic properties of material especially of polycrystalline ceramic, can be modified by doping, micro structural variation, etc.

2.7.3.1 Dielectric Constant

The overall Dielectric constant (k) of an insulator material is given by the relation

$$D = \varepsilon_0 E = \varepsilon_0 k' E \qquad \dots \qquad \dots \qquad \dots \qquad (2.25)$$

D represents the electric displacement, E the electric field in the dielectric, k the dielectric constant and ε_o permittivity of vacuum. The electric displacement describes the extent to which the electric field has been altered by the presence of the dielectric material. The dielectric constant k is an intrinsic property of a material and a measure of the ability of the material to store electric charge relative to vacuum. It is measured indirectly from the capacitance of a capacitor in which the material is used as electrode separator or dielectric. From equation 2.25 and the capacitive cell illustrated in Figure 2.15, the dielectric constant k; total charge Q (coulombs) and capacitance C (farads) can be developed as follows,

$$k' = \frac{D}{\varepsilon_0 E} = \frac{Q/A}{\varepsilon_0 V/d} \qquad \dots \qquad \dots \qquad \dots \qquad (2.26)$$

$$\text{Therefore, } Q = \varepsilon_0 k' \frac{A}{d} V \qquad \dots \qquad \dots \qquad \dots \qquad (2.27)$$

$$\text{Where, } C = \varepsilon_0 k' \frac{A}{d} \qquad \dots \qquad \dots \qquad \dots \qquad \dots \qquad (2.28)$$

$$C_0 = \varepsilon_0 \frac{A}{d} \qquad \dots \qquad \dots \qquad \dots \qquad \dots \qquad \dots \qquad (2.29)$$

$$\text{and } k' = \frac{C}{C_0} = \frac{\varepsilon}{\varepsilon_0} \qquad \dots \qquad \dots \qquad \dots \qquad \dots \qquad (2.30)$$

Here, A represents the area of the capacitive cell, d its thickness (or gap between the electrodes), Co and C the respective capacitance of the capacitor with air and material, V the voltage across the cell and the material permittivity (F/m). Thus, k' represents the ratio of the permittivity or charge storage capacity relative to air or vacuum as dielectric. It is clear from equation (2.28) that for a given size capacitor and applied voltage the

higher the k' the capacitance of the capacitor is higher. This is the only variable left with material scientist to increase the capacitance per unit volume value of capacitor for modern electronics applications.
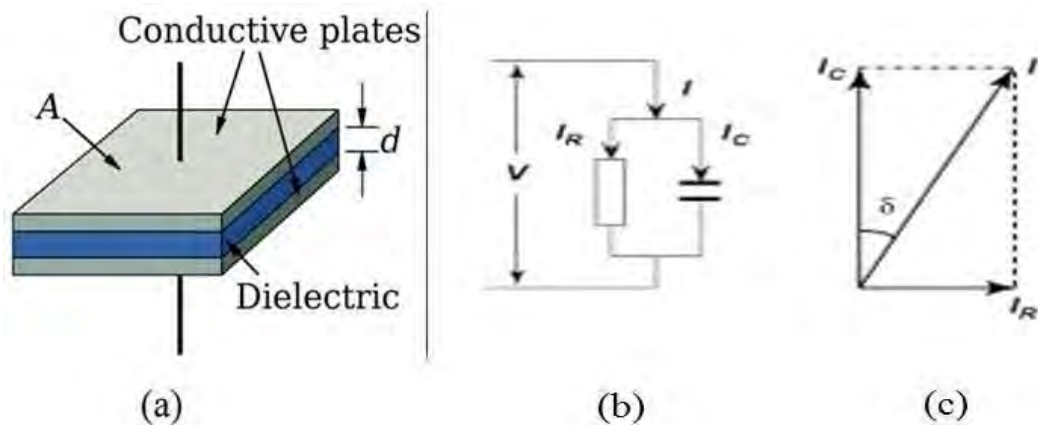
Figure 2.15: Equivalent circuit diagrams a) Capacitive cell, b) Charging and loss current c) loss tangent

2.7.3.2 Dielectric Loss

An ideal dielectric would allow on flow of electronic charge, only a displacement of charge via polarization. If a plate of such ideal material were placed between the capacitive cell shown in Figure 2.15 (a) and a DC voltage was applied, the current through the circuit would decay exponentially to zero with time. But this would not be case if an alternating (sine wave) electric field were applied. In this case the eq. 2.27 may be written as

$$Q = CV_0 e^{iwt} \qquad \dots \qquad \dots \qquad (2.31)$$

Therefore,

$$I = \frac{dQ}{dt} = i\omega CV = i\omega C_0 \varepsilon_0 k'V \qquad \dots \qquad (2.32)$$

Here, I represent the current flow on discharge of the capacitor in time t. For real dielectric material, the current I has two vector components, real I_R and imaging I_C. The condition of a lossy (not so good) dielectric illustrated in Figure 2.15 (c) as an equivalent circuit analogous of a resistance in parallel with the capacitor. I_C represent a (watt less) capacitive current proportional to the charge stored in the capacitor. It is frequency dependent and leads the voltage by 90°. On the other hand, the current I_R is ac conduction current in phase with the voltage V, which represent the energy loss or power dissipated in the dielectric. The resultant angle between the current and the voltage is Φ somewhat less than 90°. Ideal dielectric under this circumstance would not

absorb any power and the capacitor would have zero loss. The current would lead the voltage exactly 90°. The current in real capacitor lags slightly behind what it would be in an ideal capacitor. The angle of lag defined is defined as δ and the amount of lag becomes $\tan\delta$ or loss tangent.

Eq. 2.32 can be written for real and imaginary part

$$I = I_c + I_R \qquad \qquad \ldots \qquad \ldots \qquad (2.33)$$

$$= i\omega C_0 \varepsilon_0 k'V + \omega C_0 k''V \qquad \ldots \qquad \ldots \qquad (2.34)$$

By definition $\tan\delta = \left|\dfrac{I_R}{I_c}\right| \qquad \qquad \ldots \qquad \ldots \qquad (2.35)$

Dielectric loss often attributed to ion migration, ion vibration & deformation and electronic polarization is particularly important and strongly affected by temperature and frequency. The losses due to ion migration increase at low frequency and the temperature increases.

2.7.4 Dependence of dielectric properties on various factores

The property of a dielectric medium that determines the force of the electric charges, placed in the medium, exerts on each other is called dielectric constant. It is depends on the changeable external factors, such as the frequency of the voltage applied to the dielectric, temperature, frequency, particle size etc.

2.7.4.1 Dependence of dielectric constant on frequency

The process of electronic polarization in non-polar dielectric does not depend on temperature and temperature does not affect the electronic polarizability of molecules. However, due to thermal expansion of matter, the ratio of number of molecules in the effective length of the dielectric is diminishes when temperature increases and thus dielectric constant also diminishes. In solid ionic dielectric, the value of dependence of dielectric constant on temperature may be different. In most cases an ionic mechanism of polarization increases dielectric constant when the temperature grows.

However, in some cases, the value of dielectric constant may diminish when temperature rises, particularly in those substances in which ionic displacement intensifies the internal field and thereby electronic polarization. In the low temperature region, the molecules cannot in most cases orient themselves in polar dielectrics.

2.7.4.2 Dependence of dielectric constant on temperature

The dielectrics are polarized in an electric field. If switching the direction of the field, the direction of the polarization will also switch in order to align with the new field. This cannot occur instantaneously, some time is needed for the movement of charges or rotation of dipoles.

If the field is switched, there is a characteristic time that the orientational polarization (or average dipole orientation) takes to adjust, called the relaxation time. Typical relaxation times are $\sim 10^{-11}$ s. Therefore, if the electric field switches direction at a frequency higher than $\sim 10^{11}$ Hz, the dipole orientation cannot „keep up" with the alternating field, the polarization direction is unable to remain aligned with the field, and this polarization mechanism ceases to contribute to the polarization of the dielectric.

In an alternating electric field both the ionic and the electronic polarization mechanisms can be thought of as driven damped harmonic oscillators (like a mass on a spring), and the frequency dependence is governed by resonance phenomena. This leads to peaks in a plot of dielectric constant versus frequency, at the resonance frequencies of the ionic and electronic polarization modes. A dip appears at frequencies just above each resonance peak, which is a general phenomenon of all damped resonance responses, corresponding to the response of the system being out of phase with the driving force. At higher frequencies the movement of charge cannot keep up with the alternating field, and the polarization mechanism ceases to contribute to the polarization of the dielectric.

As frequency increases, the material"s net polarization drops as each polarization mechanism ceases to contribute, and hence its dielectric constant drops. At sufficiently high frequencies (above $\sim 10^{15}$ Hz), none of the polarization mechanisms are able to switch rapidly enough to remain in step with the field. The material no longer possesses the ability to polarize, and the dielectric constant drops to 1, the same as that of a vacuum.

Reference

[1]. Hans Schmid., "Multi-ferroic magnetoelectrics, Ferroelectrics", 162 (1): 317–338, 1994.

[2]. Hans Schmid., "Some symmetry aspects of ferroics and single phase multiferroics", Journal of Physics: Condensed Matter, 20 (43): 434201, 2008.

[3]. Eerenstein, W., Mathur, N. D., and Scott, J. F., "Multiferroic and magnetoelectric materials", Nature, 442 (7104): 759–765, 2006.

[4]. Ascher, E., Rieder, H., Schmid, H., and Stössel, H., "Some properties of ferromagnetoelectric nickeliodine boracite, $Ni_3B_7O_{13}I$", Journal of Applied Physics, 37(3): 1404–1405, 1966.

[5]. Nicola., Hill, A., "Why are there so few magnetic ferroelectrics?", The Journal of Physical Chemistry B, 104(29): 6694, 2000.

[6]. Wang, J., Neaton, J. B., Zheng, H., Nagarajan, V., Ogale, S. B., Liu, B., Viehland, D., Vaithyanathan, V., Schlom, D. G., Waghmare, U. V., Spaldin, N. A., Rabe, K. M., Wuttig, M., and Ramesh, R., "Epitaxial $BiFeO_3$ multiferroic thin film heterostructures", Science, 299, 1719, 2003.

[7]. Kimura, T., Goto, T., Shintani, H., Ishizaka, K., Arima., and Tokura, Y., "Magnetic control of ferroelectric polarization", Nature, 426 (6962): 55–58, 2003.

[8]. Hur, N., Park, S., Sharma, P. A., Ahn, J. S., Guha, S., and Cheong, S-W., "Electric polarization reversal and memory in a multiferroic material induced by magnetic fields", Nature, 429, 392, 2004.

[9]. Fiebig, M., "Revival of the magnetoelectric effect", Journal of Physics D: Applied Physics 38, R123, 2005.

[10]. Eerenstein, W., Mathur, N. D., and Scott, J. F., "Multiferroic and magnetoelectric materials", Nature 442, 759, 2006.

[11]. Khomskii, D. I., "Multiferroics: Different ways to combine magnetism and ferroelectricity", Journal of Magnetism and Magnetic Materials 306, 1, 2006.

[12]. Cheong, S.-W., and Mostovoy, M., "Multiferroics: a magnetic twist for ferroelectricity", Nature Materials 6, 13, 2007.

[13]. Velev, J. P., Jaswal, S. S., and Tsymbal, E. Y., "Multiferroic and magnetoelectric materials and interfaces", Philosophical Transactions of the Royal Society A: Mathematical,Physical and Engineering Sciences 369, 3069, 2011.

[14]. Prellier, W., Singh, M., and Murugavel, P., "The single-phase multiferroic

oxides: from bulk to thin film", Journal of Physics: Condensed Matter 17, R803, 2005.

[15]. Tokura, Y., and Kida, N., "Dynamical magnetoelectric effects in multiferroic oxides", Philosophical Transactions of the Royal Society A: Mathematical,Physical and Engineering Sciences 369, 3679, 2011.

[16]. Lawes, G., and Srinivasan, G., "Introduction to magnetoelectric coupling and multiferroic lms", Journal of Physics D: Applied Physics 44, 243001, 2011.

[17]. Khomskii, D., "Classifying multiferroics: Mechanisms and effects", Physics, Vo 2, 20, 2009.

[18]. Ma, J., Hu, J., Li, Z., and Nan, C.-W., "Recent Progress in Multiferroic Magnetoelectric Composites: from Bulk to Thin Films", Advanced Materials 23, 1062, 2011.

[19]. Martin, L. W., Crane, S. P., Chu, Y.-H., Holcomb, M. B., Gajek, M., Huijben, M., Yang, C.-H., Balke, N., and Ramesh, R., "Multiferroics and magnetoelectrics: thin films and nanostructures", Journal of Physics: Condensed Matter 20, 434220, 2008.

[20]. Nan, C.-W., Bichurin, M. I., Dong, S., Viehland, D., and Srinivasan, G., "Multiferroic magnetoelectric composites: Historical perspective, status, and future directions", Journal of Applied Physics 103, 031101, 2008.

[21]. Srinivasan, G., "Magnetoelectric Composites", Annual Review of Materials Research 40, 153, 2010.

[22]. Zhai, J., Xing, Z., Dong, S., Li, J., and Viehland, D., "Magnetoelectric Laminate Composites: An Overview", Journal of the American Ceramic Society 91, 351, 2008.

[23]. Martin, L., Chu, Y.-H., and Ramesh, R., "Advances in the growth and characterization of magnetic, ferroelectric, and multiferroic oxide thin films", Materials Science and Engineering: R: Reports 68, 89, 2010.

[24]. Yan, L., Yang, Y., Wang, Z., Xing, Z., Li, J., and Viehland, D., "Review of magnetoelectric perovskite-spinel self-assembled nano-composite thin films", Journal of Materials Science 44, 5080, 2009.

[25]. Hall, J.R., Hook, H.E., "Solid state physics (2nd ed.)", pp. 205–206, 1994.

[26]. Caig., Malcon Mc., John Wiley., and Sons., "Permanent Magnet in Theory and Practice", Inc. Toronto, 1977.

[27]. David Jiles., "Introduction to Magnetism and Magnetic Materials", 1st edition, Chapman & Hall, New York, 1991.

[28]. Parasnis, D. S., Harper., and Brothers., "Magnetism from Lodestone to Polar Wandering", New York, 1961.

[29]. Goldman, A., "Handbook of Modern Ferromagnetic Materials", Kulwer Acad. Pub, Boston, U. S. A., 1999.

[30]. Valenzuela, R., "Magnetic Ceramics", Cambridge University Press, Cambridge, 1994.

[31]. Yan, M. F., and Johnson, D. W., "Impurity induced exaggerated grain growth in Mn-Zn ferrites", J. Am. Ceram. Soc, Vol-61, pp 342, 1978.

[32] Kyzmin, E.V., Petrakovsky, T. A., "Physics of the magnetic order matter", Novosibirsk: Nayka, 1976.

[33] Petrakovsky, T. A., "Amorphous magnetic", Novosibirsk, 1981.

[34] Korenblit, I., Shender, E. F., "Spin glasses", Mockow: Znanie, 1984.

[35]. Carter, C. B., Norton, M. G., "Ceramic Materials Science and Engineering", Springer, New York, 2007.

Chapter 3

Sample Preparation and Experimental Techniques

3.1 Sample Preparation

3.1.1 Introduction

For quality research, it is very important to use high purity raw materials. Another vital thing during sample preparation is to remain careful so that no impurity gets incorporated into the samples. Additionally, accurate weight calculation and measurement are also important to ensure single phase formation. After sample preparation, sample characterization and property measurement is carried out and finally a relationship between structure and property is established. Finally, during all experiments starting from sample preparation to property measurement, all parameters should be maintained for getting good consistent results.

3.1.2 Powder Preparation

There exist a wide variety of methods for the synthesis of polycrystalline materials. Out of them, the solid-state reaction method is the broadly used technique for the preparation of polycrystalline solids. In this method reactants are mixed together in a powder form and heated for extended periods at high temperature. High temperature provides a considerable amount of energy to accelerate the reaction rate. Hence, the final product obtained from this method is thermodynamically stable. The major benefit of this method is the formation of structurally single phase product with desired properties which depends on final sintering temperature.

3.1.2.1 Milling

The required weight percentage of the oxide materials was calculated to be added for different compositions which were weighed with the help of electronic balance with accuracy up to 10^{-4} gms. The mixture of these oxides was crushed to fine powder in an agate mortar and pestle. The grinding continued till a homogeneous mixture was obtained.

3.1.2.2 Formation of Structure

High temperature provides the necessary energy for the reaction to occur. A solid state reaction is a direct reaction between starting reagents (usually powders) at high temperature. Solid state reaction is usually slow process because during the reaction, a large amount of bonds break and the ions migrate through a solid unlike gas phase and solution reactions. The limiting factor in solid state reaction is usually diffusion. So the rate controlling step in a solid state reaction is the diffusion of the cations through the product layer. Solid state reaction occurs much more quickly with increasing temperature and reaction does not normally occur until the reaction temperature reaches at least 2/3 of the melting point of one of the reactants.

In solid state reaction method, raw materials are weighed out according to the stoichiometry of the compound with due consideration for impurity and moisture contents. Raw materials are mechanically mixed and then grinding operations are performed to control the particle size and to mixture homogeneous. For this purpose milling operations are performed which can reduce the particle size to usually 1-10 μm range [1].

An attempt to reduce the size of the particles further may affect the homogeneity and purity of the material. Distilled water or alcohol is used as wetting medium as it is available with adequate purity at low cost and is non-inflammable. Next step is the solid state reaction between the constituents of starting materials at suitable temperature. This process is called firing or calcinations. During calcinations, control over stoichiometry is essential and for it volatile constituents have to be compensated. Calcinations causes the constituents to interact by inter diffusion the ions and resulting in a homogeneous body. Hence it is considered that calcinations are the part of the mixing process. Calcinations also control the shrinkage during sintering. After calcinations powder is compacted to give desired shape, known as green body and this green body is densified through sintering. A general discussion on calcinations and sintering are given in the next sections.

3.1.2.3 Calcination

Calcination is the process in which a material is heated to a temperature below its melting point to effect the thermal decomposition or the phase transition other than melting point, or removal of a volatile fraction. Calcination also helps in homogenizing the materials and reducing the shrinkage during the subsequent sintering process of the final shaped samples. The process of calcination derives its name from the Latin calcinare (to burn lime) [2] due to its most common application. The product of calcination is usually referred to in general as "calcine," regardless of the actual minerals undergoing thermal treatment. Calcination is differnet from roasting, in which more complex gas-solid reactions take place between the furnace atmosphere and the solids.

Synthesis of the phase of a compound takes place by solid phase reaction,which involves the chemical reaction through atomic diffusion among grains at temperature below the melting points of the raw materials [3]. Calcination reactions usually take place at or above the thermal decomposition temperature or the transition temperature (for phase transitions). In the materials which have volatile constituents , to avoid loss of the volatile parts, the calcination temperature must be kept low enough. We have calcined the samples at 800 $^{\circ}$C for 1.5 hours in a programmable furnace.

3.1.3 Shaping

Calcined powders are mixed again to give a suitable shaping to the powder. Then uniaxial pressing is used to make compacts of small sizes with simple shapes of the calcined powder. It is carried out in a die having movable top. A cavity is formed at the bottom in lower portion. This cavity is filled with free flowing granulated powder and it is stuck with the top to die. With the help of the top-punch, pressure is applied using a hydraulic press. Around one gm of powder was pressed into pellets using a hydrolic pressure and the pellets were held under the pressure for one minute using a pressing unit. After rejecting the pellets from the dies the pellets were dried. The thickness of our prepared pellets was about 1mm and the radius of the pellet was 50 mm.

3.1.4 Sintering

Process of forming objects from a metal powder by heating the powder at a temperature below its melting point. In the production of small metal objects it is often not practical to cast them. Through chemical or mechanical procedures a fine powder of the metal can be produced. When the powder is compacted into the desired shape and heated i.e., sintered, for up to three hours, the particles composing the powder join together to form a single solid object.

When thermal energy is apply to powder compact, the compact is densified and the average grain size is increases. Basic phenomena occurring from this process is densification and grain growth. This is process used to produced density control materials or compound from metal or ceramic powder by applying thermal energy. During sintering at an appreciable tempreature,the atomic motion is more violent and the area between grains in contact inverses due to the thermal espansion of the grains and finally only one interface between two grains remains.This corresponds to a state with much lower surface energy. In this state, the atoms on the grain surfaces are affected by neighbouring atoms in all directions ,which results in densified ceramics [3].

Sintering aims to produce sintered part with reproducible and if possible designed a microstructure through control the sintering variables. Microstructural control means control of gain size, sintered density, and size and distribution of other phases including pores. In most of the cases microstructural control prepare a full dense body with fine grain structure.
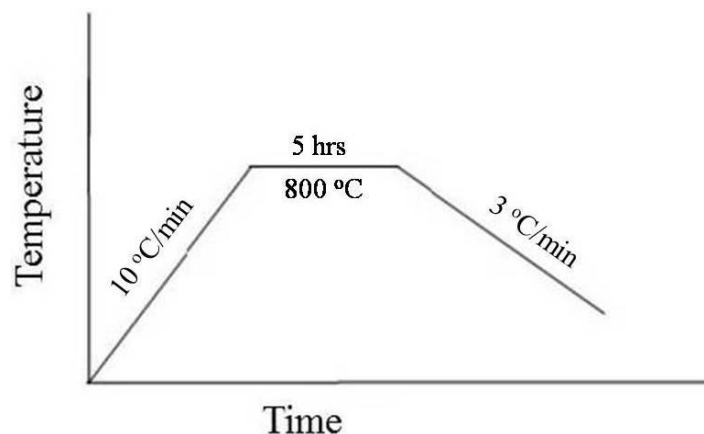
Figure 3.1: Sintering cycle diagram

The basic sintering cycles used in the experiments is shown if figure 3.1. The maximum sintering temperature, sintering rate and cooling rate were varied and which is given in figure.

3.1.5 Synthesis of Composition

There are basically four steps in the preparation of composition. They are

1. We grinded the milled powder into extremely fine powder for 4 hours.
2. The prepared powder were kept in programmable furnace for calcinations process and heated at temperature below melting point of the sample for the phase formation and removal of a volatile fraction.
3. Then we make pellets by using hydraulic pressure
4. We sintered the samples to get the structural,dielectric and magnetic properties of the ceramics.

3.1.6 Preparation of $Bi_{1-x}Gd_xMnO_3$ (x=0.00-0.12) bulk ceramics

The $Bi_{1-x}Gd_xMnO_3$ (x = 0.00-0.12) ceramics were synthesized by a standard solid state reaction technique. The high purity oxides of Bi_2O_3, Gd_2O_3, and $MnCO_3$ are taken in a stoichiometric ratio. These mixture were carefully weighed in stoichiometric proportion, mixed thoroughly with acetone and grounded in an agate mortar until a homogeneous mixture was formed. The compacted mixtures of reagents taken in desired cation ratios were calcined at 800 ^{o}C for 1.5 hours in a programmable furnace. The calcined powders were grounded again for 2 hours to get more homogeneous mixture. The powders were pressed into pellets of thickness 1 mm and diameter 12 mm by using a uni-axial hydraulic press and sintered at 825 ^{o}C for 5 hours at heating rate 10 ^{o}C per minute. The sintered pellets and powders were used to measure the required structural, morphological, dielectric and magnetic properties.

3.2 Characterization Techniques

3.2.1 X-ray Diffraction

X-ray diffraction (XRD) is a standard structural characterization technique for bulk materials. X-ray scattering techniques are a family of non-destructive analytical techniques which reveal information about the crystallographic structure, chemical

composition, and physical properties of materials. These techniques are based on observing the scattered intensity of an X-ray beam hitting a sample as a function of incident and scattered angle, polarization, and wavelength or energy. When X-rays interact with a crystalline substance (Phase), one gets a diffraction pattern. An electron in an alternating electromagnetic field will oscillate with the same frequency as the field. When an X-ray beam hits an atom, the electrons around the atom start to oscillate with the same frequency as the incoming beam. In almost all directions we will have destructive interference, that is, the combining waves are out of phase and there is no resultant energy leaving the solid sample. XRD is based on constructive interference of monochromatic X-Rays and a crystalline sample. The monochromatic X-rays are generated by a cathode ray tube, filtered to produce monochromatic radiation, collimated to concentrate them and directed toward the sample. The interaction of the incident rays with the sample produces constructive interferences (and a diffracted ray), when conditions satisfy Bragg's law.

Bragg found that crystalline solids have remarkably characteristic patterns of reflected x-ray radiation. In crystalline materials, for certain wavelengths and incident directions, intense peaks of scattered radiation were observed. Bragg accounted for this by regarding a crystal as made out of parallel planes of atoms, spaced by distance d apart. The conditions for a sharp peak in the intensity of the scattered radiation were that: (1) the x-rays should be specularly reflected by the atoms in one plane; (2) the reflected rays from the successive planes interfere constructively.
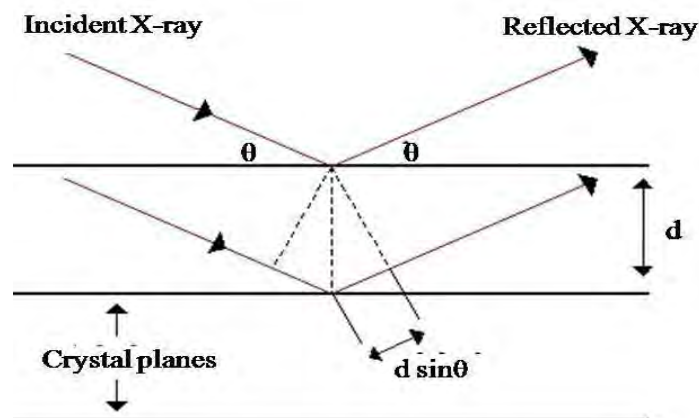
Figure 3.2: Bragg's law of diffraction

Figure shows X-rays which are specularly reflected from adjacent planes. The path difference between the two x-rays is equal to 2dsinθ. For the x-rays to interfere constructively this difference must be an integer number of wavelengths. This leads to the Bragg condition: 2dsinθ = mλ. The integer m is known as the order of the corresponding reflection (or order of interference).
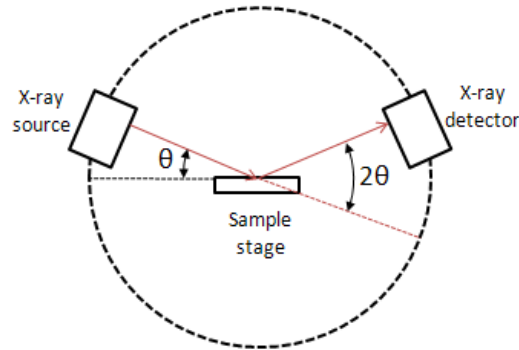
Figure 3.3: The schematic diagram shows the operation of XRD.

There are a number of various setups for studying crystal structure using x-ray diffraction. In most cases, the wavelength of radiation is fixed, and the angle is varied to observe diffraction peaks corresponding to reflections from different crystallographic planes. We have collected XRD patterns at RT using a diffractometer (Rigaku Ultimate VII) with CuK_α (α=1.5418A˚) radiation.

3.2.2 Microstructure Study

The scanning electron microscope (SEM) is a type of electron microscope that images the sample surface by scanning it with a high energy beam of electrons in a raster scan pattern. The SEM uses a focused beam of high-energy electrons to generate a variety of signals at the surface of solid specimens. The electrons interact with the atoms that make up the sample producing signals that contain information about the sample's surface topography, composition and other properties such as electrical conductivity.The electron gun at the top of the column produces a high-energy beam,which is focused into a fine spot (4 nm in diameter) on the specimen. Secondary electrons are produced on the specimen surface and are detected by a suitable detector. The amplitude of the secondary electron signal varies with time according to the topography of the specimen surface. then the signal is amplified and used to display the corresponding specimen information. Areas ranging from approximately 1

cm to 5 microns in width can be imaged in a scanning mode using conventional SEM techniques (magnification ranging from 20X to approximately 30,000X, spatial resolution of 50 to 100 nm).

Figure 3.4: JEOL JSM-5800 Scanning Electron Microscope

The SEM has a large depth of field, which allows a large amount of the sample to be in focus at one time. The SEM also produces images of high resolution, which means that closely spaced features can be examined at a high magnification. Preparation of the samples is relatively easy since most SEMs only require the sample to be conductive. The types of signals produced by an SEM include secondary electrons, back-scattered electrons (BSE), characteristic X-rays, light (cathode-luminescence), specimen current and transmitted electrons. Essential components of all SEMs include the following:

- Electron Source ("Gun")
- Electron Lenses
- Sample Stage
- Detectors for all signals of interest
- Display / Data output devices
- Infrastructure Requirements:
  - Power Supply
  - Vacuum System
  - Cooling system

o   Vibration-free floor

o   Room free of ambient magnetic and electric fields
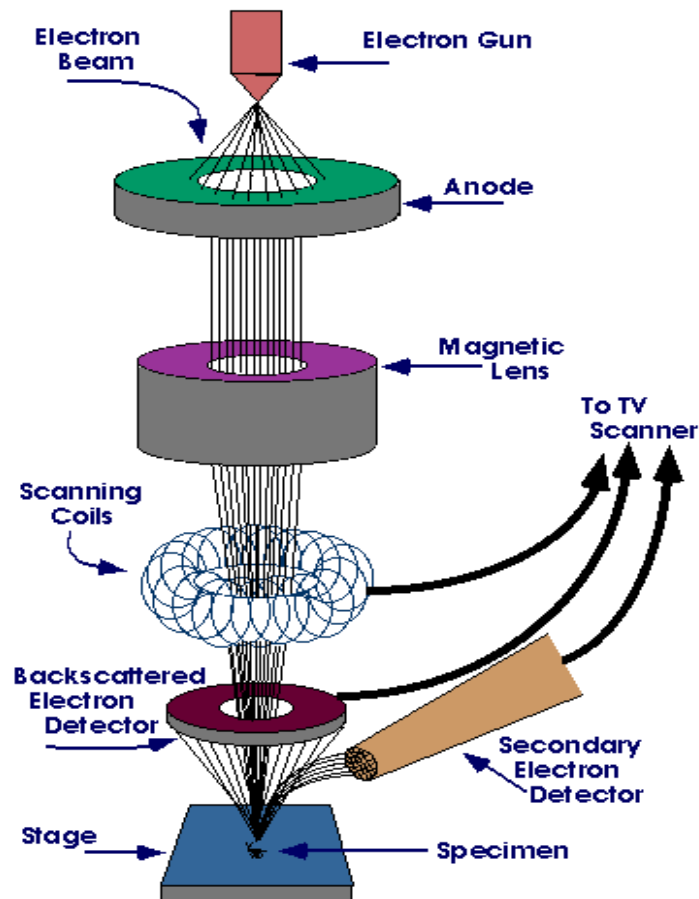
Figure 3.5: Schematic diagram of Scanning electron microscope [4].

SEMs always have at least one detector (usually a secondary electron detector), and most have additional detectors. The specific capabilities of a particular instrument are critically dependent on which detectors accommodate it. The microstructral study of the samples was performed in order to get an insight of the grain structures. Average grain diameter of the samples was determined by linear intercept technique [5].

However, the practical resolution depends on the properties of the specimen, the specimen preparation technique, and also on many instrumental parameters, such as the beam intensity, accelerating voltage, scanning speed, distance of the lens from the specimen's surface, and the angle of the specimen with respect to the detector. Under optimum conditions a resolution of 1 nm can be achieved. We have used Field Emission Scanning Electron Microscope (FESEM) in this experiment. In Field

emission, we need less temperature to gain electron gun and have better resolution in it as compare to SEM.

3.2.3 X-ray Photoelectron Spectroscopy (XPS)

X-Ray Photoelectron Spectroscopy (XPS) was developed in the mid 1960's by K. Siegbahn and his research group from the University of Upsalla, Sweden [6, 7]. The technique is based on the photoelectric effect outlined by Einstein in 1905 and is a failure analysis technique primarily used in the identification of elements from the sample surface. The analysis is done by irradiating a sample with soft X-rays to ionize atoms and releasing core-level photoelectrons. The usually used radiations are those of aluminium (Al K-alpha E = 1.487 keV) and magnesium (Mg K-alpha E = 1.254 keV). Although X radiations penetrate deep into the sample, the important information regarding the electronic structure of the solid is given only by those electrons who manage to reach the surface without any energetic loss due to inelastic scattering processes. A rigorous description of photoemission process implies a quantum description of this process which consists in the emission of an electron from the inner shells of a solid, the detection of the photoelectron is made after it leaves the sample surface. The most known theoretical model of the photoemission process is the so called "three-step model" developed Spicer in 1985 [8]. In 1964 Berglund and Spicer, published a more sophisticated formalization of the same model [9]. Along the time there were developed many theories that tried to explain the photoemission process, in present the most used of them is the one known as "one step model". XPS can detect all elements except H and He (owing to the absence of the core orbital).

An XPS spectrum is displayed as a plot of electron binding energy versus the number of electrons in a fixed energy interval and can be divided in two parts:
• primary spectrum – generated by the electrons that are leaving the solid without suffering inelastic scattering processes
• secondary spectrum (background) – formed by the photoelectrons who have lost a percentage of their kinetic energy due to inelastic scattering processes

There are various spectral features that are likely to be encountered in a XPS spectrum. Some are fundamental to the technique, and are always observed, and

others are dependent upon the chemical and physical nature of the sample. Valence band levels appear as lines of low intensity in the low binding energy region of the XPS spectrum, between the Fermi level and about 10-15 eV binding energy. These energetic levels are very important in explaining the properties of solids because one can determine the band structure considering only the direct transitions that can happen without any other external excitation. XPS measures the transitions between these occupied and the unoccupied states and offer important information about the occupied states in the valence band region. The Fermi level position gives us information about vacant states from the valence band and curve's slope near Fermi level is a measure of the states density. The electrons from the most inner shells of the atoms give rise to the most intense and well define lines in the XPS spectrum. A closer inspection of the spectrum shows that emission from some levels does not give rise to a single photoemission peak, but a closely spaced doublet, due to spin-orbit splitting. The exact binding energy of an electron depends not only upon the level from which photoemission is occurring, but also upon: formal oxidation state of the atom, local, chemical and physical environment. Changes in these states give rise to small shifts in the peak positions so-called chemical shifts [10]. In the photoemission process the photon kicks out the electron so quickly that the remaining electrons do not have time to readjust. The reorganization of the electrons upon the core-hole can lead to electronically excited final states. This means that the XPS spectrum will consist from the main line which corresponds to the lowest excited state and a number of additional lines, so called satellites, which correspond to the higher excited state after the photoemission.

The spectrometer is built up from: a control computer, electronic control units, a "quick-entry" system and a main and preparation chamber. The bulk samples were crushed in situ in the preparation chamber in high–vacuum conditions (usually around 7×10^{-8} torr), in order to prevent surface contamination, and then transferred to the main chamber where the measurements were performed. A quick–entry system is also available allowing a rapid, convenient, and direct introduction of samples into the main chamber. The main components of the spectrometer, which is situated in the main chamber, are sketched in Figure-3.6.
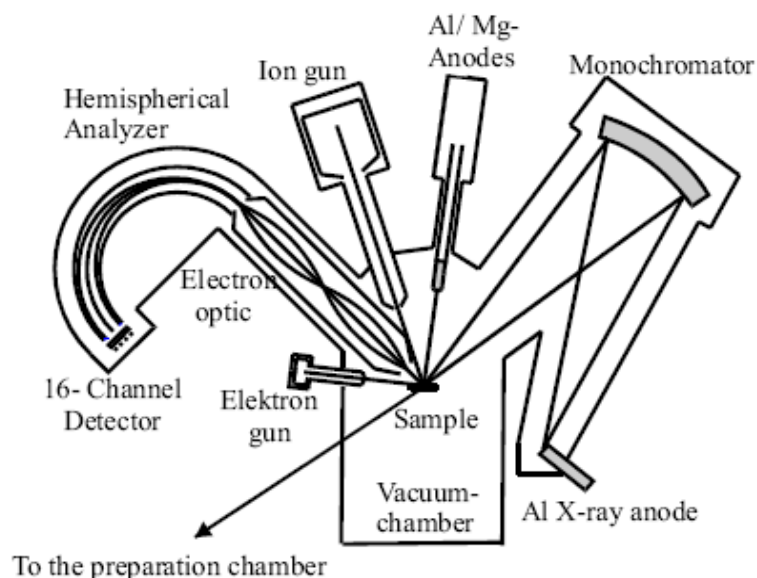
Figure 3.6: Schematic diagram of the PHI 5600 spectrometer

For insulating samples a low-energy electron gun can be used to compensate the superficial local charges accumulated on the surface. The accelerating potential can be chosen between 0 and 10 V at a maximal current of 25 μA. All components of the main chamber ware kept under UHV during the experiments. There are two important reasons why ultra–high vacuum (UHV) conditions are requested when performing XPS measurements. In order for the photoelectrons to reach the analyzer without being scattered by gas molecules a basic vacuum in the 10^{-5} torr range is required. However under such a pressure the surface of the sample is quickly contaminated. In order to avoid surface contamination during the measurements, which can take up to several hours, a base pressure of about 10^{-10} torr must be ensured. UHV conditions are reached by employing a combination of appropriate turbo molecular, sputter and sublimation vacuum pumps. During the recording of the XPS spectra presented in this work the base pressure in the main chamber was maintained below 1×10^{-9} torr.

3.2.4 Dielectric Property Measurement

A dielectric is an electrical insulator that may be polarized by the action of an applied electric field. A common example of a dielectric is the electrically insulating material between the metallic plates of a capacitor. The polarization of the dielectric by the

applied electric field increases the capacitor's surface charge for the given electric field strength.

An impedance analyzer (Agilent 4294A) was used to measure the dielectric property of samples. Measurements of the samples were done as a function of frequency and temperature.

First of all samples were prepared properly to measure dielectric properties correctly. Samples were kept clean and dry. They were polished with 120 grit paper in order to produce crack free solid sample. Samples were given geometrical shape commonly circular in order to measure the area. Sample thickness was kept quite uniform which was essential for correct measurement. For the measurement of dielectric properties the samples will be painted on either side with silver paste to ensure good electric contacts. Next the samples were kept in the holder of the impedance analyzer to measure the properties. The measure frequency was varied from 10Hz to 100MHz. Experimental set up is shown in Figure 3.7.
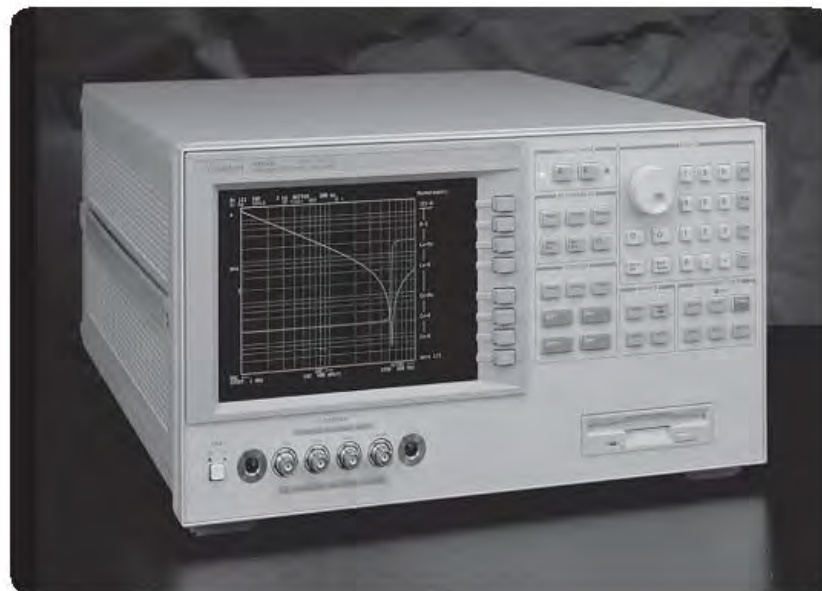
Figure 3.7: Agilent 4294A Impedance Analyzer

Measurements of dielectric properties normally involve the measurements of the change in caacitance and loss of a capacitor in presence of the dielectric materials. The behavior of a capacitance can now be described as follows. Here an ideal loss less air capacitor of capacitance C_0. On insertion of a dielectric material in a space the

capacitance will be changed.The dielectric constant (ε_r) and electrical properties measurements on disk-spaced specimens will be carried out at room temperature on all the samples in the high frequency range. The dielectric constant ε_r will be calculated using the following relations,

$$\varepsilon_r = \frac{C \times t}{\varepsilon_o \times A}$$

where C is the measured capaciatance of the sample, t is thickness of the capacitor and A is the area of cross section of the disk space sample and ε_0 is the permitivity of the free space (8.854 X 10^{-12} F/m).

3.2.5 Magnetic Property Measurement

There are various means of measuring magnetization of a substance. The magnetization of a substance is usually determined by measuring its magnetic moment divided by the volume or mass of the substance. In the present study magnetization has been performed using a Vibrating Sample Magnetometer (VSM) and a Superconducting Quantum Interface Device (SQUID) magnetometer. A VSM was used to measure the field and temperature dependence of the magnetization in order to determine the transition temperature and the value of the spontaneous magnetization at 0 K by extrapolation. A SQUID magnetometer was used to measure the magnetic susceptibility in field cooled (FC) and zero field cooled (ZFC). The basic principle of magnetic measurements follows Faraday's law. As the second law states that the change of magnetic flux with time would generate a voltage which is proportional to rate of change of flux.

3.2.5.1 Vibrating Sample Magnetometer (VSM)

VSM developed by S. Foner [11, 12] is a versatile and sensitive method of measuring magnetic properties and is based on the flux change in a coil when the sample is vibrated near it. The VSM is an instrument designed to continuously measure the magnetic properties of materials as a function of temperature and field. In this type of magnetometer, the sample is vibrated up and down in a region surrounded by several pickup coils. The magnetic sample is thus acting as a time-changing magnetic flux, varying inside a particular region of fixed area.

VSM is used to measure the magnetic properties of the sample. The basic principle of VSM lies on Faraday's Law of Induction, $\nabla \times \vec{E} = \dfrac{\partial \vec{B}}{\partial t}$ which tells us that a changing magnetic field (B) will produce an electric field (E). This electric field can be measured and can give us information about the changing magnetic field. Thus, the sample is placed in a constant magnetic field and oscillated with a fixed frequency near a set of detection (pickup) coils. If the sample is magnetic, the constant magnetic field induces a magnetic dipole moment in the sample. This magnetic dipole moment creates a magnetic field around the sample. As the sample is oscillated, this magnetic flux changes as a function of time and the voltage induced (proportional to the rate of change of flux) in the pickup coils is synchronously detected. The voltage will also be proportional to the magnetic moment of the sample. In Figure-3.6, we show (a) schematic of VSM and (b) detailed configuration near the pick-up coils. The system detection capability can be maximized by optimizing the geometry of the pickup coils and by having oscillation amplitude that is relatively large (1 − 3 mm peak). The time dependent voltage induced in the pickup coils is given by

$$V_{induced} = \frac{d\varphi}{dt} = \frac{d\varphi}{dz}\frac{dz}{dt}$$

where, φ represents the magnetic flux, the axis of oscillation of the sample is conventionally chosen to be the z–axis, and z, therefore, represents the position of the sample along this axis and t is the time. If the sample is made to oscillate sinusoidally, then the induced voltage in the pickup coils will have the form $V_{induced} = cmA\omega \sin \omega t$, where, c is a coupling constant, m is the DC magnetic moment of the sample, A is the amplitude of oscillation, and $\omega = 2\pi f$, where f is the frequency of oscillation of the sample. The detection of the magnetic moment of the sample, thus, amounts to measuring the coefficient of sinusoidal voltage response induced in the detection coil. In our laboratory, we have used a VSM, Lakeshore, model 7407 series (with maximum filed strength 1.6 T and minimum achievable temperature of 80K) to measure the magnetic properties of the samples.
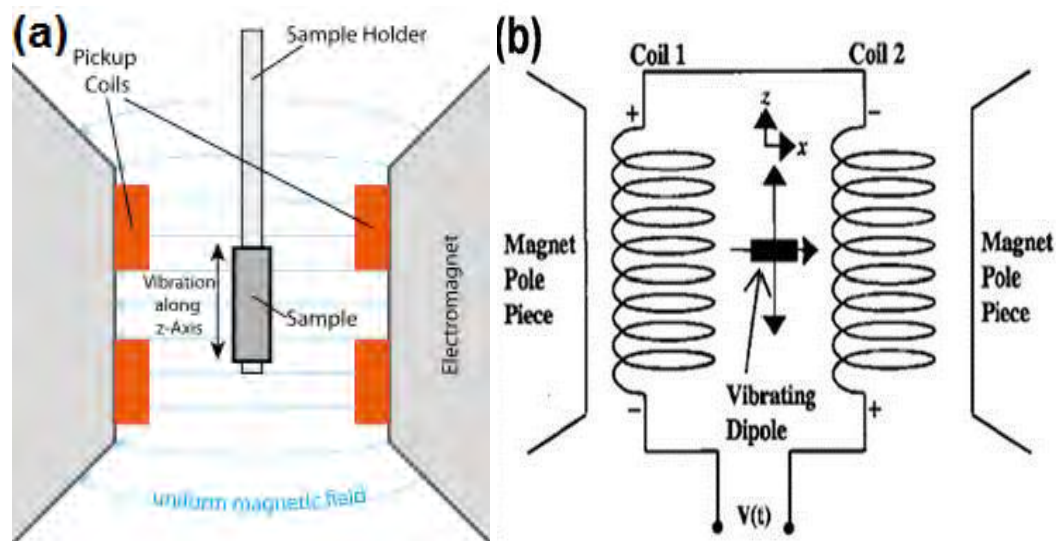
Figure 3.8: Schematic diagram of (a) VSM and (b) details near the pickup coils.

3.2.5.2 Super-conducting Quantum Interference Device (SQUID) Magnetometer

SQUID is another-type of magnetometer which has much higher sensitivity ($\sim10^{-8}$ emu) compared to the VSM ($\sim10^{-8}$ emu). Thus SQUID magnetometer provides the opportunity to measure the sample having very low magnetic moment with high degree of accuracy. The basic principle of a SQUID is based on the quantum interference of wave functions that describe the state of the superconducting charge carriers (the Cooper pairs). A SQUID is based on an interferometer loop in which two weak links (Josephson contacts) are established. A weak link is established by interrupting a superconductor by a very thin insulating barrier. The function of the SQUID is to link the quantum mechanical phase difference of the Cooper pairs wave functions over a weak link with the magnetic flux penetrating the interferometer loop [13, 14].

The major components of a SQUID magnetometer are: superconducting magnet, superconducting detection coil, a SQUID connected to the detection coil, superconducting magnetic shield. Superconducting magnets are solenoid made of superconducting wire which must be kept at liquid helium dewar. The uniform magnetic field is produced along the axial cylindrical bore of the coil. The superconducting pick-up coil system, which is configured as a second order

gradiometer is placed in the uniform magnetic field region of the solenoidal superconducting magnet.
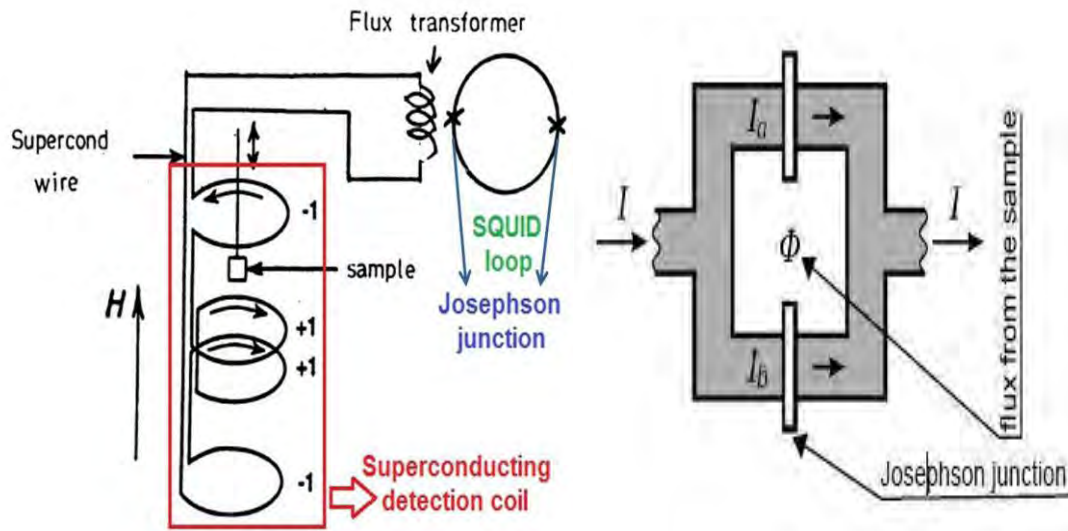
Figure 3.9: Schematic diagram of SQIUD magnetometer

The SQUID device is usually a thin film that functions as an extremely sensitive current to voltage converter. Measurements are done in this equipment by moving the samples through the second order gradiometer. Hence, the magnetic moment of the sample induces an electric current in the pick-up coil system. Superconducting magnetic shield is used to shield the SQUID sensor from the fluctuations of the ambient magnetic field of the place where the magnetometer is located and from the large magnetic field produced by the superconducting magnet.

Using this kind of equipment we can measure the real and imaginary components of AC magnetic susceptibility as a function of frequency, temperature, AC magnetic field amplitude and DC magnetic field, and time. It is an important feature of the instrument that one can change the magnetic field either by "oscillate mode" or "no overshoot mode". The oscillate mode is used to minimize the remanent field of the magnet, whenever an accurate value of magnetic field is needed, e.g. in case of zero field cooling. In the hysteresis measurement the no overshoot mode has been selected, in which the field is changed directly from one value to another, and the magnet is returned to its persistent mode.

References

[1]. Moulson, A. J., and Herbert, J. M., "Electrocermics Materials, Propertics and Application", Chapman & Hall, UK, 1990.

[2]. Mosby's Medical., "Nursing and Allied Health Dictionary, Fourth Edition", Mosby-Year Book Inc.,p. 243; 1994.

[3]. Xu, Y., "Ferroelectric Materials and Their Applications", Elsevier Science Pub Co, New York, USA, 1991.

[4]. http://www.purdue.edu/ehps/rem/rs/sem.htm.

[5]. ASTM E112: Standard Test Methods for Determining Average Grain Size.

[6]. Sigbahn, K., Nordling, C., Fahlman, A., Nordberg, R., Hamrin, K., Hedman, J., Johansson, G., Bergmark, T., Karlsson, S.E., Lindgren, I., ESCA-Atomic, "Molecular and Solid State Structure Studied", by Means of Electron Spectroscopy, Almquist and Wicksell, Uppsala, 1967.

[7]. Sigbahn, K., Nordling, C., Johansson, G., Hedman,J., Heden, P.F., Harmin, K., Gelius, U., Bergmark, T., Werme, L.O., Manne, R., Baer, Y., "ESCA Applied to free molecules", North Holland Amsterdam, 1969.

[8]. Spicer, W.E., "Photoemissive, Photoconductive and Optical Absorption Studies of Alkali-Antimony Compounds", Phys. Rev. 112, 114, 1958.

[9]. Berglund, N., and Spicer, W. E., "Photoemission Studies of Copper and Silver: Theory", Phys. Rev. 136, A1044, 1964.

[10]. Hüfner, S., "Photoelecron Spectroscopy Principles and Applications", Springer-Verlang, Berlin, 1995.

[11]. Foner, S., "Versatile and Sensitive Vibrating-Sample Magnetometer", Rev. Sci. Instr., 30, 7, 1959.

[12]. Foner, S., Rev. Sci. Instr., 27, 578, 1955.

[13]. Jaklevic, R. C., Lambe, J., Silver, A. H., and Mercereau, J. E., "Quantum Interference Effects in Josephson Tunneling", Phys. Rev. Letters 12 (7): 159–160, 1964.

[14]. Cappella, B., and Dietler, G., "Force distance curves by atomic force microscopy", Surface Science Reports 34, 1-104, 1999.

Chapter 4

Results and Discussion

In this investigation, the nominal composition of $Bi_{1-x}Gd_xMnO_3$ (x = 0.00-0.12) ceramics were synthesized by conventional solid state reaction technique. The morphological, dielectric and magnetic properties of undoped $BiMnO_3$ and Gd doped $BiMnO_3$ were investigated. The outcome of this investigation was described in this chapter.

4.1 XRD analysis

The structural properties of the synthesized ceramics was studied at room temperature by XRD using CuK_α (α=1.5418 Å) radiation. Figure 4.1 (a) and (b) shows the XRD pattern of $Bi_{1-x}Gd_xMnO_3$ (x=0.00-0.12) ceramics synthesized by solid state reaction technique. From the figure all picks were not viable to identify but some picks were identified. However, the picks which have been identified are relevant with the previous investigation and confirm the monoclinic structure [1, 2] of the prepared ceramics.
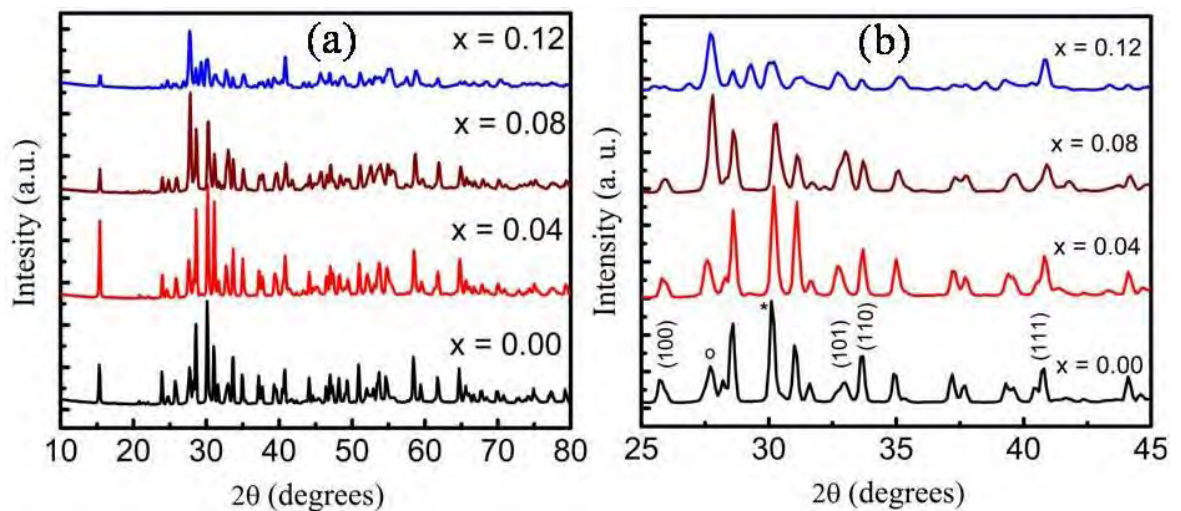
Figure 4.1: X-ray diffraction patterns of $Bi_{1-x}Gd_xMnO_3$ (x=0.00-0.12) ceramics are shown in figure (a). The enlarge view of the pattern are shown in figure (b), asterisk and open circle indicates the impurity phases.

The XRD peaks of the samples are mainly consists of $BiMnO_3$, with contamination by bismuth oxycarbonate ($Bi_2O_2CO_3$) and traces of $Bi_2Mn_4O_{10}$. The formation of secondary impurity peaks is apparently unavoidable during the synthesis of ceramic materials using solid state reaction technique [1].

4.2 Microstructure Development

The surface morphology of $Bi_{1-x}Gd_xMnO_3$ (x=0.00-0.12) ceramics was investigated by a field emission scanning electron microscopy (FESEM) imaging. The FESEM images are shown in figure 4.2 (a-d) and their corresponding histograms (figure (e-h)) demonstrate the grain size distribution of all compositions. From the micrographs, it is observed that the average grain size decreases significantly with the increase of Gd concentration.

From the FESEM image of figure 4.2 (a) and its corresponding histogram figure 4.2 (e), the average grain size of undoped $BiMnO_3$ sample is ranging from 500 nm to 1200 nm. Upon substitution of 4% Gd in place of Bi in $BiMnO_3$, the average grain size is reduced and varied from 250 nm to 500 nm as shown in figure 4.2 (b) and its respective histogram (figure 4.2 (f)). For a further substitution of 8 % Gd, the grain size distribution becomes much narrower that is varied from 250 nm to 350 nm as shown in figure 4.2 (c) and its respective histogram are in figure 4.2 (g). Finally the substitution of 12 % Gd reduced the average size and varied from 180 nm to 280 nm with a very narrow distribution of their sizes. This was demonstrated in FESEM image 4.2 (d) and its respective histogram figure 4.2 (h). The ionic radius of Gd^{3+} ion (0.938 Å) is quite smaller than that of Bi^{3+} (1.17 Å) which might be a reason to decrease the grain size due to the substitution of Gd in place of Bi in $BiMnO_3$. Although other reasons, in particular, the concentration of oxygen vacancies and the diffusion rate of the ions upon substitution of Gd should also be considered [3].
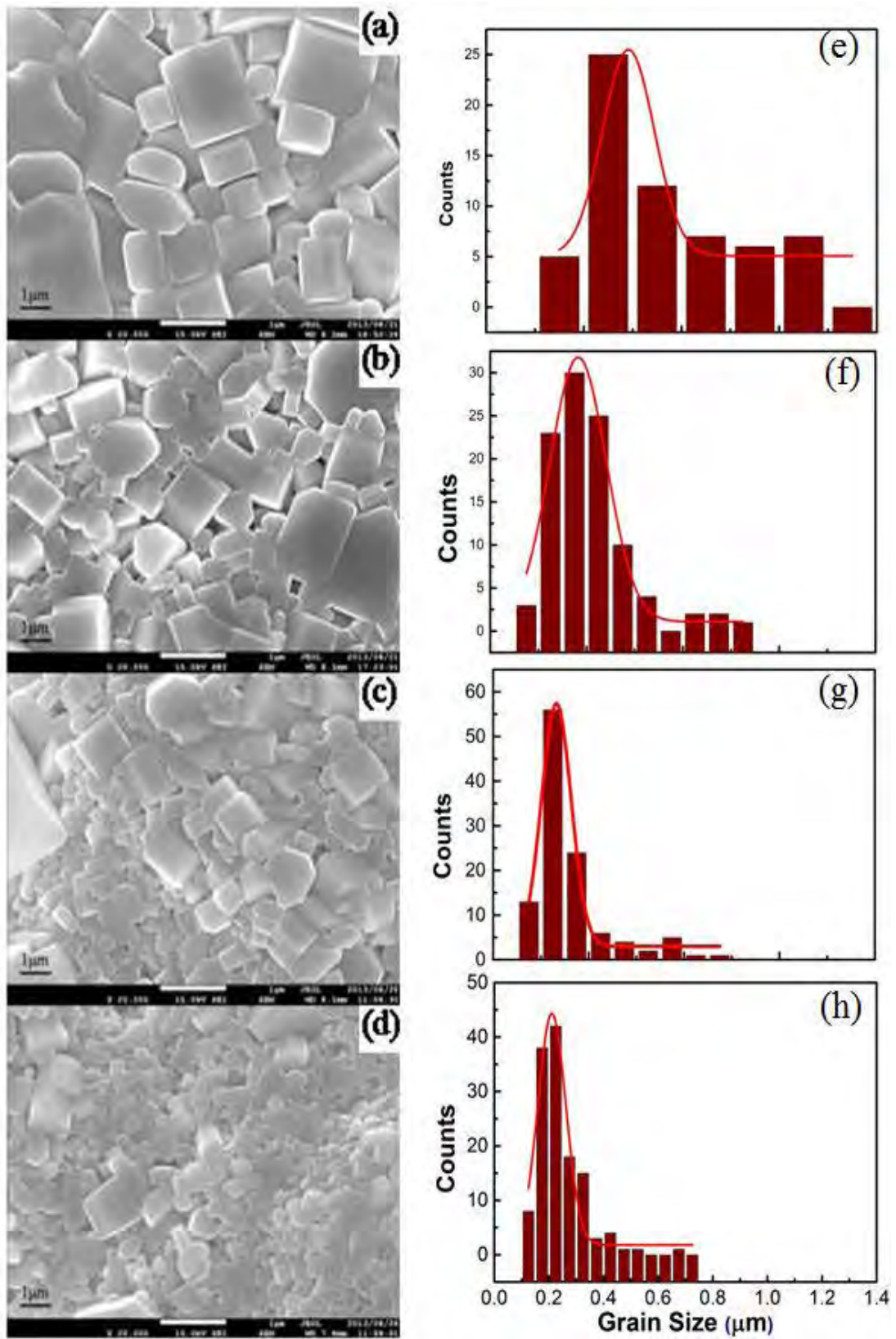
Figure 4.2: FESEM micrograph of $Bi_{1-x}Gd_xMnO_3$ ceramics: (a) x = 0.00, (b) x = 0.04, (c) x = 0.08 and (d) x = 0.12 and their corresponding histograms are shown in figure.

However, the findings clearly demonstrate that the substitution of Gd controlled the volatilization of Bi and reduced the grain growth. Previous investigations revealed that the decrease in grain size increases the grain boundary region and hence, increases the resistivity of the material [4]. Therefore, in the next stage of this investigation it is interested to measure their dielectric properties. Prior to do that the concentration of oxygen vacancies were estimated as oxygen vacancies play also a significant role in determining the electrical properties of multiferroic materials.

4.3 XPS analysis

To investigate the elemental compositions, phase impurities and to confirm the concentration of oxygen vacancies of $Bi_{1-x}Gd_xMnO_3$ (x = 0.00- 0.12) ceramics XPS measurements were carried out. The XPS survey is displayed in figure 4.3 (a), where all the characteristic peaks of the XPS spectra are well resolved. The binding energy values of Bi, Gd, Mn and O confirmed the phase purity of the compounds. Figure 4.3 (b), (c) and (d) show separately the spectrum of the 4d state of Gd, 4d and 4f states of Bi, respectively. Upon the substitution of Gd the binding energy values of the corresponding peaks were unaltered which is a good indication from phase structure point of view of this ceramic system. However, there is a small shift of splitting between Bi $4f_{7/2}$ and Bi $4f_{5/2}$ peaks that may be related to enhancement of the polarization [5-7].
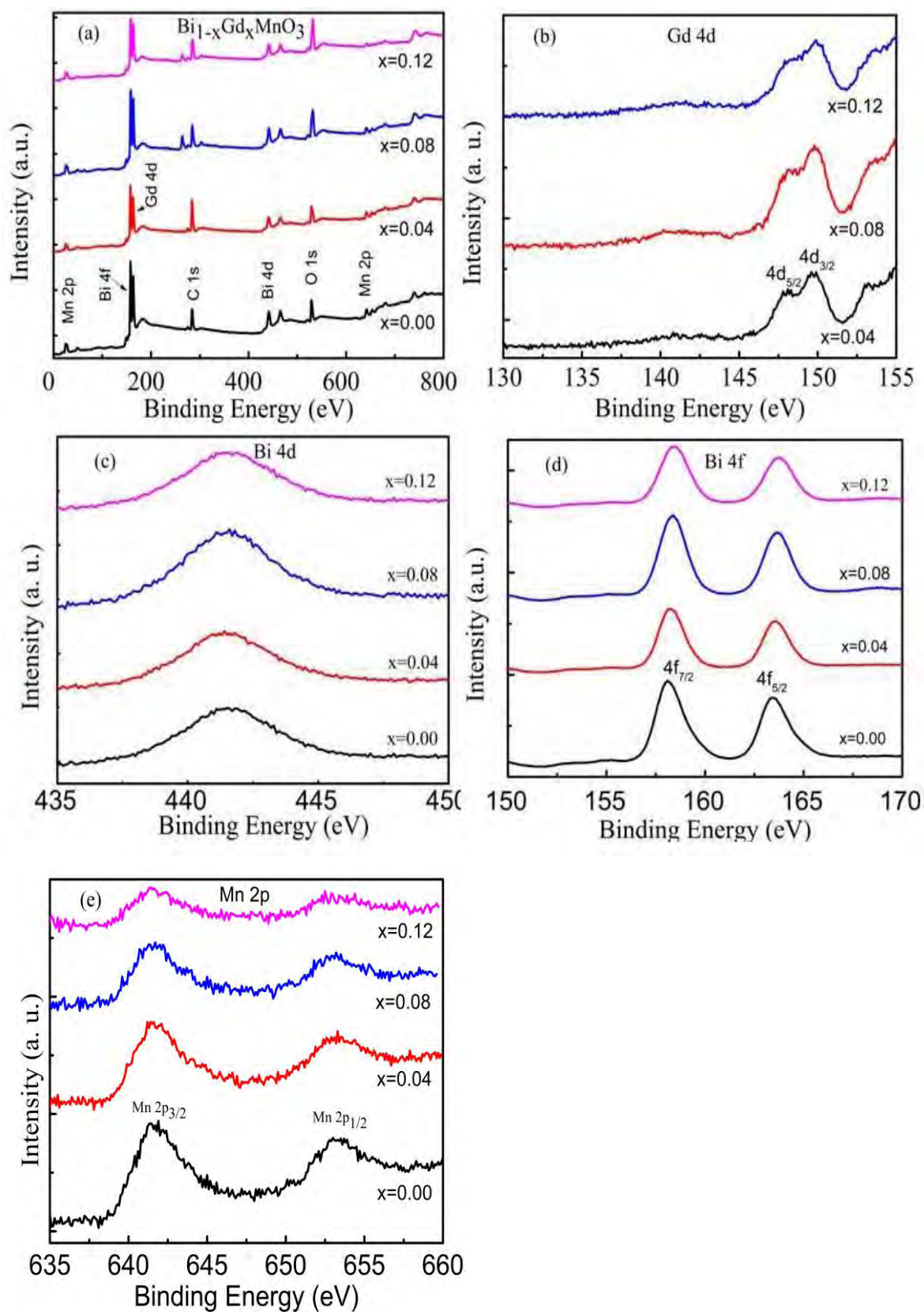
Figure 4.3: (a) XPS spectra of $Bi_{1-x}Gd_xMnO_3$ (x = 0.00- 0.12) ceramics, (b) Gd 4d level, (c) Bi 4d level, (d) Bi 4f level and (e) Mn 2p level.

Figure 4.3 (e) shows the Mn 2p spectrum of all compositions which are resolved into two peaks with lower binding energy (LBE) of 641.4 and higher binding energy (HBE) of 653.2 eV. These two binding energies with an energy gap of around 11.8 eV are correspond to Mn $2p_{3/2}$ and Mn $2p_{1/2}$, respectively [8]. The gap between these two peaks are almost unchanged, however, due to the substitution of 8 % and 12 % Gd, the peak intensity of the HBE peak was slightly reduced. This change may be related with the conversion of some of the Mn^{3+} to Mn^{4+} in the Gd substituted compositions [9].
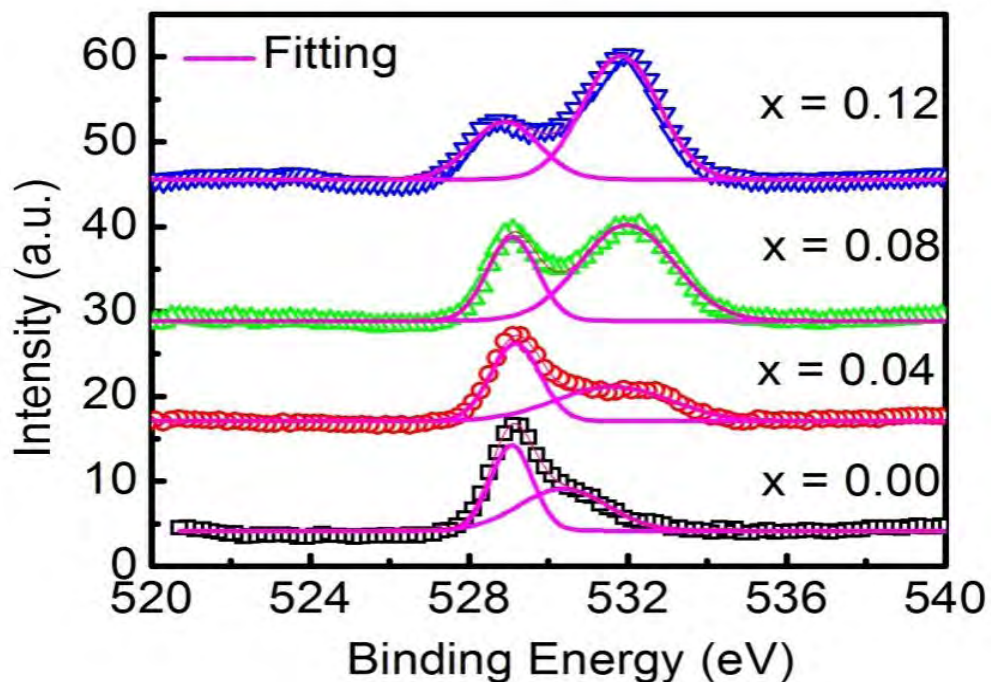
Figure 4.4: The O 1s core spectrum and oxygen vacancy peaks for all compositions.

Figure 4.4 shows the O 1s XPS spectra of $Bi_{1-x}Gd_xMnO_3$ (x = 0.00- 0.12) ceramics. The spectrum displays an asymmetric peak very close to 529 eV along with an additional peak at slightly HBE. The additional HBE peak shifted to the rightward direction and became much prominent compared to the Gd undoped sample. The asymmetric curves of the samples can be Gaussian fitted by two symmetrical peaks. The LBE peak around 529.3 eV is correspond to the O 1s core spectrum, while the HBE peak is related to the oxygen vacancy [10-13] in the samples. The area ratio of the two peaks (HBE/ LBE) are 1.66, 1.76, 1.82 and 2.03 for x = 0.00, 0.04, 0.08 and 0.12, respectively. Comparing the area ratio of HBE peak to the LBE peak, it is clear

that the area ratio increases with increasing Gd concentration. This indicates the higher concentration of oxygen vacancies in the Gd doped $BiMnO_3$ samples compared to undoped $BiMnO_3$.

4.4 Dielectric properties

Dielectric property measurements of all the samples were carried out at room temperature within a frequency range of 20Hz–20MHz. Figure 4. 5 (a) illustrates the frequency dependence of the dielectric constant of $Bi_{1-x}Gd_xMnO_3$ ceramics with (a) x = 0.00, (b) x = 0.04, (c) x = 0.08 and (d) x = 0.12 measured at RT. The variation of dielectric loss tangent (tanδ) in the same frequency range is shown in figure 4.5 (b). Both dielectric behavior and dielectric loss of the samples exhibit frequency dependence and shows dielectric dispersion.

The dielectric constant of Gd undoped sample $Bi_{1-x}Gd_xMnO_3$ (x = 0.00) is maximum at the lower frequencies which decreases sharply with increasing frequency up to about 10^4 kHz and then becomes almost constant at higher frequencies $>10^4$ kHz. The Gd undoped $BiMnO_3$ ceramics demonstrate clear dispersion at low frequency and both doped and undoped samples shows a frequency independent behavior at high frequencies ($> 10^4$ kHz).

At low frequencies, the space charges are able to follow the frequency of the applied field, while at a high frequency they may not have time to build up and undergo relaxation [4], giving a low value of dielectric constant. The effect of space charge polarization is discussed by Maxwell [14] and Wagner [15] and is good agreement with Koops phenomenological theory [16]. Beside space charge polarization, at low frequency, the dielectric constant depends on the excitation of bound electrons, lattice vibrations and dipole orientation [17], that means all contribution play an active role to determine the value of the dielectric constant.

The low frequency dispersion is also related with the increased oxygen vacancies as was observed from the XPS measurements of this ceramic system. Due to high concentration of oxygen vacancies the low frequency dispersion is common in dielectric and ferroelectric materials [18, 19].
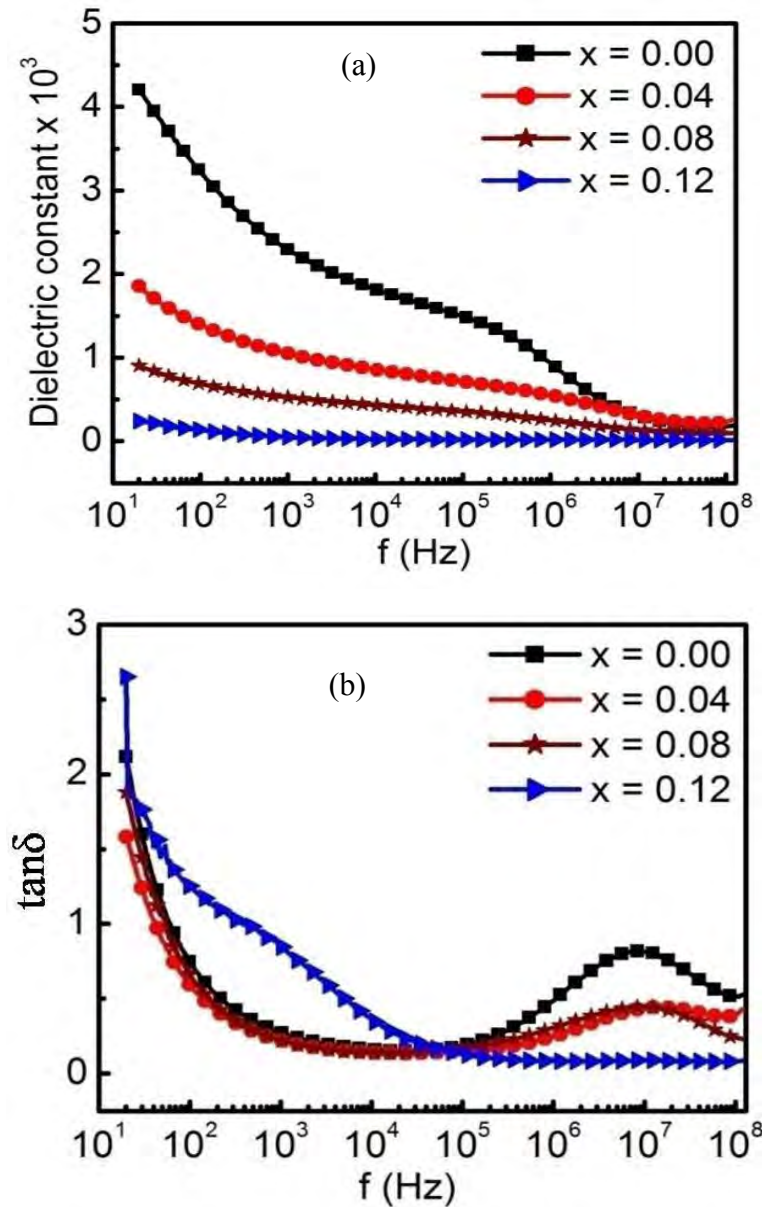
Figure 4.5 (a) Semi-log plot of dielectric constant of $Bi_{1-x}Gd_xMnO_3$ ceramics: (a) x = 0.00, (b) x = 0.04, (c) x = 0.08 and (d) x = 0.12 recorded at RT in the wide frequency range from 10Hz to 200MHz. (b) Variation in tanδ as a function of frequency at RT.

Compared to the undoped sample, the low frequency dispersion is much less in Gd doped $BiMnO_3$ ceramics. Particularly, the dielectric constant is almost constant and stable over a wide range of frequency for 12% Gd doped $BiMnO_3$ ceramic. Notably, the value of dielectric constant is higher throughout the frequency range in undoped $BiMnO_3$ ceramic. The substitution of Gd minimized the low frequency dispersion; however, the overall dielectric constant was reduced. This is unexpected as we had seen from the FESEM micrographs (figures 4.2 (a-h)) that upon the substitution of Gd

the grain size is decreased with a narrow distribution of their sizes. It is well known fact that decrease in the grain size increases the grain boundary region and hence, increases the resistivity of the material [20-23]. Therefore, we expected a higher dielectric constant due to the substitution of Gd in place of Bi in $BiMnO_3$ ceramics. It is observed that due to the presence of a significant amount of oxygen vacancies; the dielectric constant of the Gd doped ceramics was gradually decreased although they have uniform microstructure along with well-connected grains. In a previous investigation [24], it was observed that the introduction of oxygen and oxygen vacancies can lead to a reduction in dielectric constant of $BiFeO_3$ and this is in good agreement with our experimental observation.

The dielectric loss tangent also shows frequency dependency as illustrated in figure 4.5 (b). At low frequency, the dielectric loss is large and gradually decreasing with the increase of frequency for all the samples up to an intermediate frequency and shows minimum dielectric loss. After this intermediate frequency the dielectric loss is still minimum for 12% Gd substitution but for x = 0.00, 0.04 and 0.08 dielectric loss is increased with frequency, which can be introduced from the relaxation of charge carrier trapped among the oxygen vacancy [25] and resonance. This ionic relaxation comes from oxygen vacancies and it's a high frequency phenomenon from thermally activated hoping of ions. At high frequency dielectric loss is decreased. Due to the low loss tangent values at higher frequencies, the 12% Gd substituted sample might have potential applications in high-frequency microwave devices.

4.5 Magnetic properties

In the present study magnetization measurements were performed using a VSM and also SQUID magnetometer. VSM was used to measure the field dependence of the magnetization. A SQUID magnetometer was used to measure the temperature dependent magnetic property in ZFC and FC processes. In this section, the outcome of the field dependent and temperature dependent magnetization experiments were described.

4.5.1 Magnetic properties using VSM

To investigate the magnetic property of the samples magnetization versus magnetic fields hysteresis loops were carried out at room temperature (RT). Figure 4.6 shows M-H curves for undoped $BiMnO_3$ and Gd doped $Bi_{1-x}Gd_xMnO_3$ (x = 0.04-0.12) ceramics measured at RT with an applied magnetic field of up to ±12 kOe.
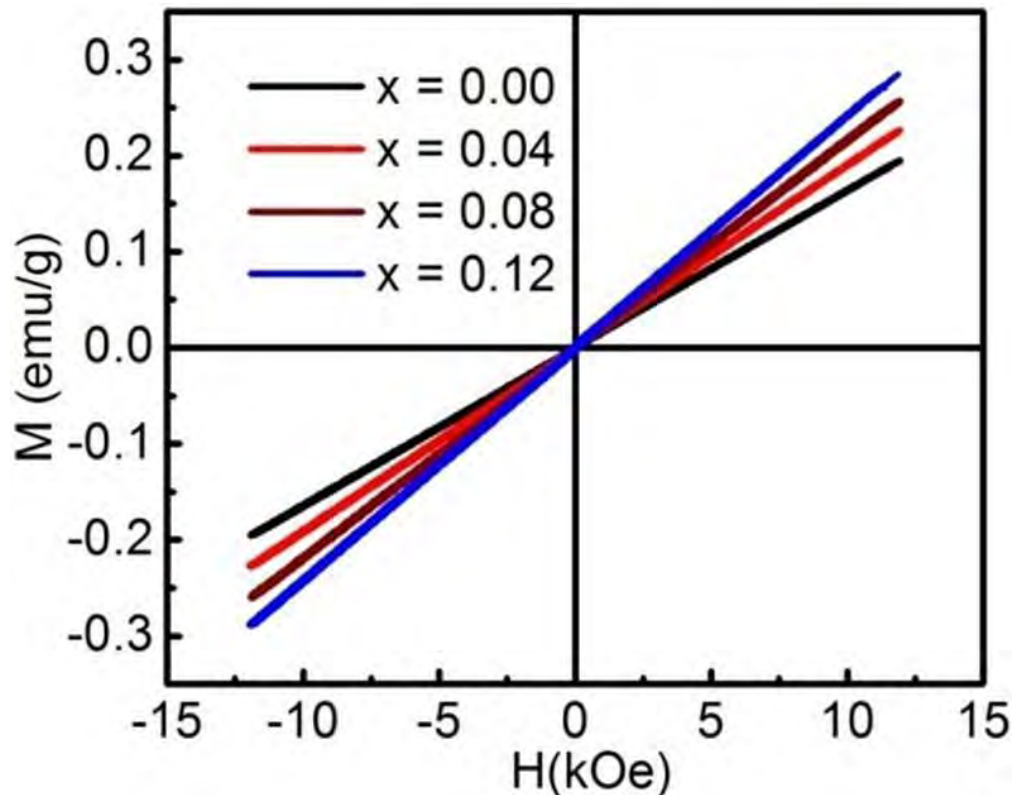
Figure 4.6: M-H loops of $Bi_{1-x}Gd_xMnO_3$ (x=0.00-0.12) ceramics at room temperature.

It is clear that all the samples show unsaturated magnetization loops upon the application of a magnetic field of up to ±12 kOe. Figure 4.7 (a) shows the enlarge view of undoped $BiMnO_3$, that is the hysteresis loop with a remanent magnetization o 0.0015 emu/g and a coercive field of ~110 Oe at RT. This is due to the fact that undoped $BiMnO_3$ is paramagnetic at room temperature and does not possess any spontaneous magnetization [1]. Figures 4.7 (b)–4.7 (d) demonstrate an enlarged view of the low-field M-H hysteresis loops of $Bi_{1-x}Gd_xMnO_3$ ceramics measured at RT with (b) x = 0.04 (c) x = 0.08 (d) x = 0.12.
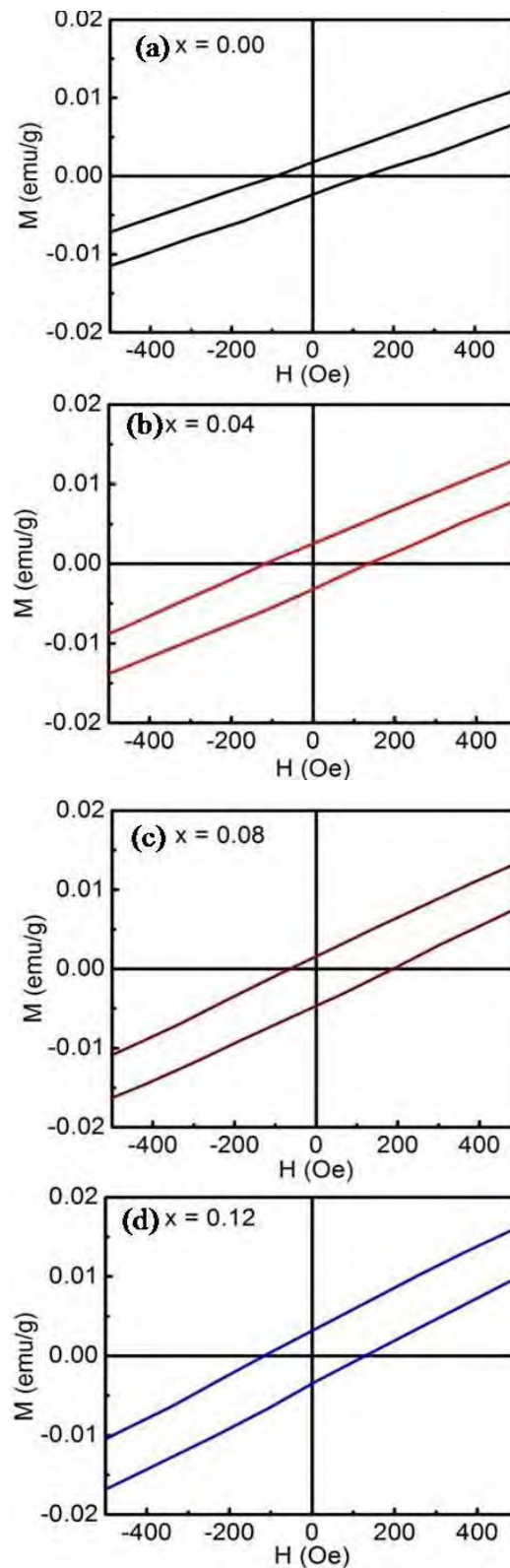
Figure 4.7: An enlarge view of the low-field M-H hysteresis loop of pure $BiMnO_3$. (a)-(d) An enlarge view of the low-field M-H hysteresis loop of $Bi_{1-x}Gd_xMnO_3$ samples obtained at RT: (b) x = 0.04, (c) x = 0.08 and (d) x = 0.12. An asymmetric shift both in the field and magnetization axes of Gd doped samples (a)-(d) indicates the existence of the EB phenomenon.

From these M-H hysteresis loops, the remanent magnetization (M_r) was calculated using the equation: $M_r = \left|(M_{r1} - M_{r2})\right|/2$ where M_{r1} and M_{r2} are the magnetization with positive and negative points of intersection with H = 0, respectively [26]. The coercive field (H_c) was given by $H_c = \left|(H_{c1} - H_{c2})\right|/2$, where H_{c1} and H_{c2} are the left and right coercive fields [27, 28] respectively. Calculated values of M_r and H_c were plotted in figure 4.8 for $Bi_{1-x}Gd_xMnO_3$ (x = 0.00-0.12) ceramics as a function of Gd concentration.

Figure 4.8: Variation of (a) remanent magnetization and (b) coercive fields at RT in $Bi_{1-x}Gd_xMnO_3$ (x=0.00-0.12) ceramics as a function of Gd concentration.

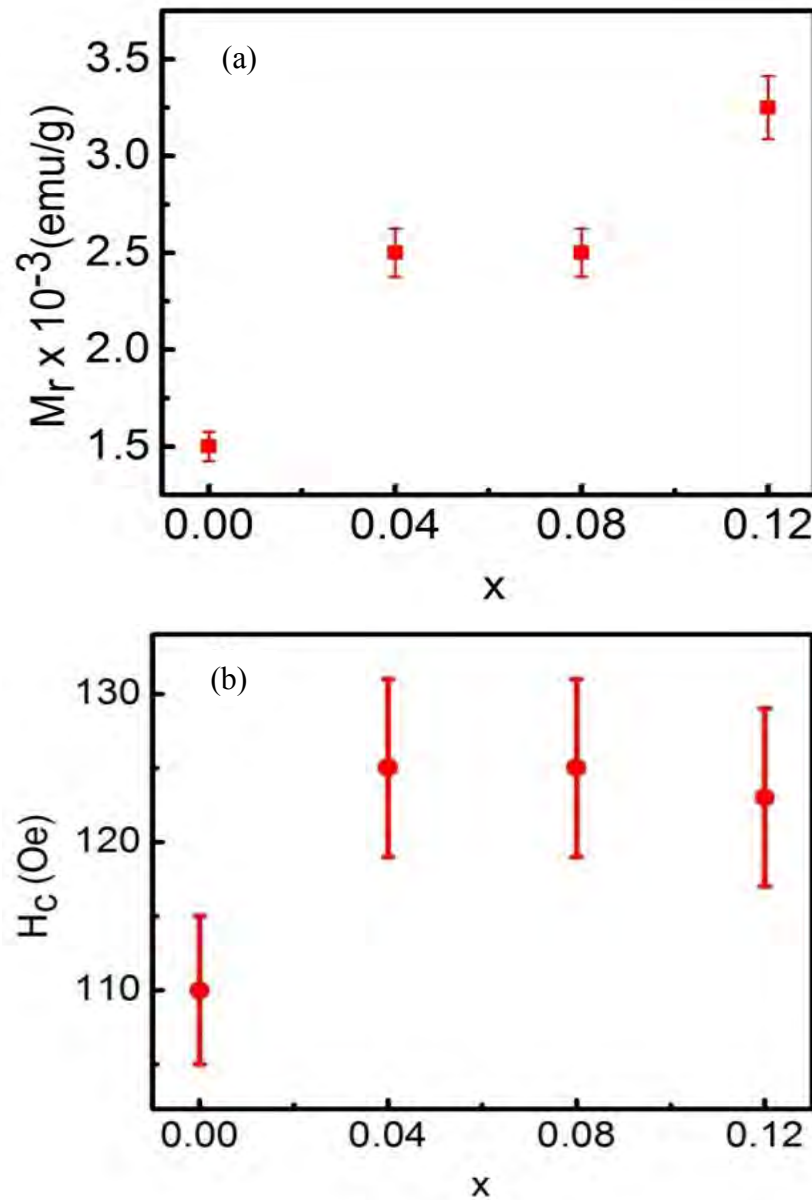An increment of Gd concentration in place of Bi in $Bi_{1-x}Gd_xMnO_3$ increased the remenant magnetization and coercive fields compared to the undoped sample. This enhancement of the magnetization at RT may be associated with the structural distortion in the perovskite with change in Mn–O–Mn bond angle. Similar results of enhancement of magnetization are observed with change in Fe–O–Fe angle in $BiFeO_3$ multiferroics [4].

In the case of Gd doped $Bi_{1-x}Gd_xMnO_3$ ceramics, the hysteresis loops of Gd doped ceramics were not really saturated at 12 kOe, however, a nominal enhancement in remanent magnetization was observed with the increase of Gd concentration in the system. The coercive fields are also increased around 15 Oe with Gd substitution but it is almost constant for 4% to 12% Gd doping concentration. It may claim that upon substitution of Gd, the magnetic properties of this ceramic system were increased compared to the undoped $BiMnO_3$, however, considering the large effective moment of Gd (8 Bohr magneton) the increment is quite nominal.

It is well known that the magnetic properties of rare earth based mixed valence perovskite manganites $R_{1-x}A_xMnO_3$ (R = La, Gd, Pr, Nd, Sm etc and A = Sr, Ba and Ca) are understood in terms of Zener double exchange (DE) mechanism [29]. In Zener DE model, the magnetic interaction is commonly thought to be the result of exchange between Mn^{3+} and Mn^{4+} ions via an oxygen ion which actually involves simultaneous transfer of e_g electron from the Mn^{3+} to the oxygen and from the oxygen to the neighbouring Mn^{4+} [29]. Moreover, in these manganite systems the conversion of Mn^{3+} to Mn^{4+} is significantly increased by oxygen vacancies [30].

On the contrary, the origination of magnetic properties in Bi based manganites like $BiMnO_3$ is not mainly responsible on double exchange interaction [31]. The magnetic properties of Bi based manganites is attributed to the presence of highly polarizable $6s^2$ lone pair of electrons present in the Bi atom, which strongly decreases the mobility of e_g electrons [31, 32]. It is anticipate that despite having large oxygen vacancies in this material system, the lone pair of Bi atoms is likely to hindrance the enhanced magnetic properties of this material system at room temperature.

TABLE : The table shows the calculated value of H_{EB} and M_{EB} for $Bi_{1-x}Gd_xMnO_3$ (x = 0.00-0.12) ceramics.

Gd Concentration (x)	$Bi_{1-x}Gd_xMnO_3$ ceramics at RT	
	H_{EB} (Oe)	M_{EB} x 10^{-4} (emu/g)
0.00	-17.5	-5.00
0.04	-10	-5.00
0.08	-62	-0.15
0.12	-7	-2.50

Beside the enhanced room temperature magnetic properties in Gd doped $Bi_{1-x}Mn_xO_3$ ceramics, the most interesting feature observed from the enlarged view (figure 4.7(a)–4.7(d)) of the low-field M-H hysteresis loops is their asymmetric behavior. An asymmetry exhibiting shifts both in the field and magnetization axes can be clearly observed for all the samples. This indicates the presence of exchange bias (EB) effect in these compounds. The exchange bias effect usually occurs in ferromagnetic and antiferromagnetic bilayers or multilayers in which the two coercive fields of the magnetic hysteresis loop are not symmetric, and the centre of the magnetic hysteresis loop shifts to the left or right [27, 28, 33]. Recent investigations also demonstrate that the exchange bias effect can also exist in compounds or composites which allow the coexistence of both a ferromagnetic component and an antiferromagnetic component [27, 28, 34]. A recent investigation [35] reported that it is possible to observe EB effect in multiferroic material system without necessarily cooling the sample through the Neel temperature T_N.

The EB field (H_{EB}) and EB magnetization (M_{EB}) can be calculate from the coercive field and remanent magnetization of a hysteresis loop. The H_{EB} is generally defined as $H_{EB} = -(H_{c1} + H_{c2})/2$, where H_{c1} and H_{c2} are the left and right coercive fields [36]. The asymmetry in the magnetization axes is defined as $M_{EB} = (M_{r1} + M_{r2})/2$, where M_{r1} and M_{r2} are the magnetization with positive and negative points of intersection with H=0, respectively [36]. For different doping concentration of Gd in

Bi1-xGd$_x$MnxO3 (x=0.00-0.12) ceramics at RT the calculated values of H$_{EB}$ and M$_{EB}$ are inserted in table 1.

It should be noted here that the present indication just provide an indication about the presence of exchange bias effect in this material system. However, to observe a tunable exchange bias field cooling experiments might be performed particularly at temperature below the phase transition temperature of this ceramic system [35].

4.5.2 Magnetic properties using SQUID

To investigate the phase transition temperature of Bi$_{1-x}$Gd$_x$MnO$_3$ ceramic system, the temperature dependent magnetization measurements were carried out using a SQUID magnetometer.

To perform the experiment in the ZFC process, the sample was initially cooled from 300K to 5K in zero field and data were collected while heating in the presence of the applied field. On the other hand, in the FC mode, data were collected while cooling in the presence of 500 Oe magnetic fields. Figure 4.9 (a) shows the temperature dependent ZFC and FC curves upon the application of a magnetic field of 500 Oe. The temperature dependent ZFC and FC magnetization curves clearly demonstrate a ferromagnetic to paramagnetic transition at 45 K.
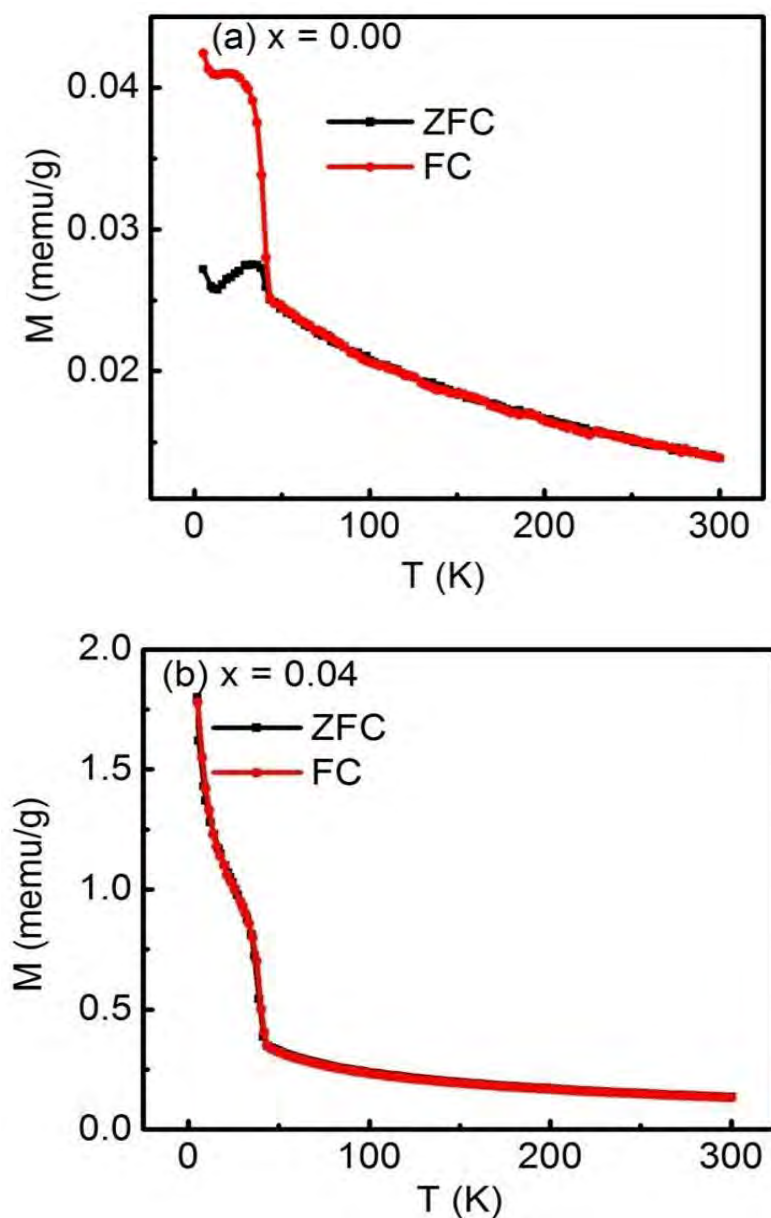
Figure 4.9: Temperature dependence of the magnetization for $Bi_{1-x}Gd_xMnO_3$ showing zero field cooling (ZFC) and field cooling (FC) curves for (a) x=0.00 and (b) x=0.04.

Below this ferromagnetic phase transition (< 37-42 K), there is a clear splitting between ZFC and FC magnetization curves. The splitting between ZFC and FC curves may be attributed to the appearance of spin-glass like behavior induced by competition between the ferromagnetic and antiferromagnetic exchange interaction [27, 37]. The spin glass state is in fact an inhomogeneous magnetic state which represents a magnetic disorder and obviously a common phenomenon in a number of magnetic systems [38, 39].

Figure 4.9 (b) demonstrates the temperature dependent ZFC and FC curves of 4 % Gd doped BiMnO$_3$ ceramic system. Unlike the magnetization curves of undoped material, here due to the doping of 4 % Gd both ZFC and FC curves were coincided with each other. From figure 4.9 (b), the ferromagnetic transition is still obvious, however, there was an upturn of magnetization curves below the phase transition temperature. The ZFC and FC curves are overlapped in Bi$_{0.96}$Gd$_{0.04}$MnO$_3$ for a wide range of temperature, indicate the response of the material in applied field is dominated by the strong magnetic behaviour of Gd^{3+} ion [40, 41].

References:

[1] Erica Montanari, Lara Righi, Gianluca Calestani, Andrea Migliori, Edmondo Gilioli and Fulvio Bolzoni, "Room Temperature Polymorphism in Metastable $BiMnO_3$ Prepared by High-Pressure Synthesis", Chem. Mater., 2005, 17, 1765, 2005.

[2] Kimura, T., Kawamoto, S., Yamada, I., Azuma, M., Takano, M. and Y. Tokura, "Magnetocapacitance effect in multiferroic $BiMnO_3$", Phys. Rev. B 67, 180401, 2003.

[3] Brinkman, K., Iijima, T., Nishida, K., Katoda, T. and Funakubo, H., "The influence of acceptor doping on the structure and electrical properties of sol-gel derived $BiFeO_3$ thin films"; Ferroelectrics, 35, 357, 2007.

[4] Uniyal, P., Yadab, K. L., "Study of dielectric, magnetic and ferroelectric properties in $Bi_{1-x}Gd_xFeO_3$", Mater. Lett. 62, 2858, 2008.

[5] Simon, V., Bako-Szilagyi, H., Neumann, M., Chiuzbaian, S.G., and Simon, S., "Atomic environment in lead-bismuth glasses containing manganese", Mod. Phys. Lett. B 17, 291, 2003.

[6] Honma, T., Benino, Y., Komatsu, T., Sato, R., and Dimitrov, V., "Correlation among electronic polarisability, optical basicity, interaction parameter and XPS spectra of Bi_2O_3-B_2O_3 glasses", Phys. Chem. Glasses 43, 2002.

[7] Fan, H., Hu, L., Yang, K. and Fang, Y., "Structure and physical properties of Bi_2O_3–B_2O_3–Ga_2O_3 glasses", J. Non-Cryst. Solids 356, 1814, 2010.

[8] Liu, D., Zhang, Q., Xiao, P., Garcia, B. B., Guo, Q., Champion, R., Cao, G., "Hydrous Manganese Dioxide Nanowall Arrays Growth and Their Li^+ Ions Intercalation Electrochemical Properties" Chem. Mater. 20, 1376, 2008.

[9] Elena Konysheva and John T. S. Irvine, "Evolution of conductivity, structure and thermochemical stability of lanthanum manganese iron nickelate perovskites", J. Mater. Chem. 18, 5147, 2008.

[10] Fang, L., Liu, J., Ju, S., Zheng, F., Dong, W. and Shen, M., ", Experimental and theoretical evidence of enhanced ferromagnetism in sonochemical synthesized $BiFeO_3$ nanoparticles,", App. Phys. Lett. 97, 242501, 2010.

[11] Das, R., Sarkar, T. and Mandal, K., "Multiferroic properties of Ba^{2+} and Gd^{3+} co-doped bismuth ferrite: magnetic, ferroelectric and impedance spectroscopic analysis", J. Phys. D: Appl. Phys., 45, 455002, 2012.

[12] Tian, J., Gao, H., Kong, H., Yang, P., Zhang, W. and Chu, J. "Influence of transition metal doping on the structural, optical, and magnetic properties of

TiO_2 films deposited on Si substrates by a sol–gel process", Nanoscale Research Letters, 8, 533, 2013.

[13] Rath, C., Mohanty, P., Pandey, A. C., and Mishra, N. C., "Oxygen vacancy induced structural phase transformation in TiO_2 nanoparticles", J. Phys. D: Appl. Phys., 42, 205101, 2009.

[14] Maxwell, J. C., "Electricity and Magnetism", Vol. 1 (Oxford University Press, Oxford, 1929) Section 328.

[15] Wagner, K. W., "Zur theorie der unvoll Kommener dielektrika", Ann. Phys. (Leipzig) 40, 817, 1913.

[16] Koops, C. G., "On the Dispersion of Resistivity and Dielectric Constant of Some Semiconductors at Audiofrequencies", Phys. Rev. 83, 121, 1951.

[17] Samantaray, S., Mishra, D. K, Pradhan, S. K., Mishra, P., Sekhar, B. R., Debdhyan Behera, Rout, P. P., Das, S. K., Sahu, D. R and Roul, B. K, "Correlation between structural, electrical and magnetic properties of $GdMnO_3$ bulk ceramics" Journal of Magnetism and Magnetic Materials, 339, 168, 2003.

[18] Hu, G. D., Cheng, X., Wu, W. B. and Yang, C. H., "Effects of Gd substitution on structure and ferroelectric properties of $BiFeO_3$ thin films prepared using metal organic decomposition"Appl. Phys. Lett. 91, 232909, 2007.

[19] Inas Kamal Batttisha, Ibrahim Sayed Ahmed Farag, Mostafa Kamal, Mohamed Ali Ahmed, Emad Girgis, Hesham Azmi El Meleegi, Fawzi El Desouki, "Dielectric and Magnetic Properties of Nano-Structure $BiFeO_3$ Doped with Different Concentrations of Co Ions Prepared by Sol-Gel Method", New Journal of Glass and Ceramics, 5, 59, 2015.

[20] Khomchenko, V. A., Kiselev, D. A. Vieira, J. M., Kholkin, A. L., Sa, M. A., and Pogorelov, Y. G., "Synthesis and multiferroic properties of $Bi_{0.8}A_{0.2}FeO_3$ (A = Ca, Sr, Pb) ceramics", Appl. Phys. Lett. 90, 242901, 2007.

[21] Liu, J., Li, M., Pei, L., Yu, B., Guo, D. and Zhao, D. X., "Effect of Ce doping on the microstructure and electrical properties of BiFeO3 thin films prepared by chemical solution deposition", J. Phys. D: Appl. Phys. 42, 115409, 2009.

[22] Wang, Y., and Nan, C-W. "Effect of Tb doping on electric and magnetic behavior of $BiFeO_3$ thin films", J. Appl. Phys. 103, 024103, 2008.

[23] Idrees, M., Nadeem, M., Atif, M., Siddique, M., Mehmood, M. and Hassan, M.M., "Origin of colossal dielectric response in $LaFeO_3$", Acta Mater. 59, 1338, 201.

[24] Lou Yan-Hui, Song Gui-Lin, Chang Fang-Gao and Wang Zhao-Kui, "Investigation on dependence of $BiFeO_3$ dielectric property on oxygen content", Chin. Phys. B 19, 077702, 2010.

[25] Makhdoom, A. R., Akhtar, M. J., Rafiq, M. A., Hassan, M. M. "Investigation of transport behavior in Ba doped $BiFeO_3$" Ceramics International 38, 3829, 2012.

[26] Anjum, G., Kumar, R., Mollah, S., Shukla, D. K., Kumar, S. and Lee, C. G., "Structural, dielectric, and magnetic properties of $La_{0.8}Bi_{0.2}Fe_{1-x}Mn_xO_3$ ($0.0 \leq x \leq 0.4$) multiferroics", J. App. Phys. 107, 103916, 2010.

[27] Guo, Y., Shi, L., Zhou, S., Zhao, J., Wang, C., Liu, W. and Wei, S., "Tunable exchange bias effect in Sr-doped double perovskite La_2NiMnO_6", J. Phys. D: Appl. Phys. 46, 175302, 2013.

[28] Muthu, S. E., Singh, S., Thiyagarajan, R., Selvan, G. K., Rao, N. V. R., Raja, M. M. and Arumugam, S., "Influence of Si substitution on thestructure, magnetism, exchange bias andnegative magnetoresistance in $Ni_{48}Mn_{39}Sn_{13}$ Heusler alloys", J. Phys. D: Appl. Phys. 46, 205001, 2013.

[29] Coey, J. M. D., Viret, M., "Mixed-valence manganites" Advances in Physics 48, 167, 1999.

[30] Wang Z. L., Kang Z. C., "Functional and Smart Materials, Structural Evolution and Structure Analysis", Plenum Press, New York, Chapter 8, page 441, 1998.

[31] Garca-Munoz, J. L., Frontera, C., Aranda, M. A. G., Ritter, C., Llobet, A., Respaud, M., Goiran, M., Rakoto, H., Masson, O., Vanacken, J., and Broto, J. M., "Charge and orbital order in rare-earth and Bi manganites: a comparison" Journal of Solid State Chemistry 171, 84, 2003.

[32] Rao, S. S., Bhat, S. V., "Preparation, Characterization, and Magnetic Studies of $Bi_{0.5}X_{0.5}(X = Ca, Sr) MnO_3$ Nanoparticles " J. Nanosci. Nanotechnol. 7, 2025, 2007.

[33] Hong, F., Cheng, Z., Wang, J., Wang, X. and Dou, S., "Positive and negative exchange bias effects in the simple perovskite manganite $NdMnO_3$", Appl. Phys. Lett. 101, 102411, 2012.

[34] Yoshii, K., "Positive exchange bias from magnetization reversal in $La_{1-x}Pr_xCrO_3$ ($x \sim 0.7$–0.85)", Appl. Phys. Lett. 99, 142501, 2011.

[35] Basith, M. A., Khan, F. A., Bashir Ahmmad, Shigeru Kubota, Fumihiko Hirose, Ngo, D.-T., Tran, Q.-H. and Mølhave, K. "Tunable exchange bias effect in magnetic

$Bi_{0.9}Gd_{0.1}Fe_{0.9}Ti_{0.1}O_3$ nanoparticles at temperatures up to 250K" J. Appl. Phys 118, 023901, 2015.

[36] Basith, M. A., Kurni, O., Alam, M. S., Sinha, B. L. and Bashir Ahmmad, "Room temperature dielectric and magnetic properties of Gd and Ti co-doped $BiFeO_3$ ceramics" J. Appl. Phys.115, 024102, 2014.

[37] Nesic, M. P., Stanojevic, Z. M., Brankovic, Z., Cotic, P., Bernik, S., Goes, M. S., Marinkovic, A., Varela, J.A., Brankovic, G., "Mechanochemical synthesis of yttrium manganite" J. Alloys Comp. 552, 451, 2013.

[38] Vijayanand, S., Mahajan, M. B., Potdar, H. S., and Joy, P. A. "Magnetic characteristics of nanocrystalline multiferroic $BiFeO_3$ at low temperatures", Phys. Rev. B 80, 064423, 2009.

[39] Stanojevic, Z. M., Brankovic, Z., Jaglicic, Z., Jagodic, M., Mancic, L., Bernik, S., Recnik, A., Brankovic, G., "Structural and magnetic properties of nanocrystalline bismuth manganite obtained by mechanochemical synthesis", J. Nanopart. Res. 13, 3431, 2011.

[40] Negi, P., Dixit, G., Agrawal, H. M., Srivastava, R. C., "Structural, Optical and Magnetic Properties of Multiferroic $GdMnO_3$ Nanoparticles", J Supercond Nov Magn 26, 1611, 2013.

[41] Zhu Jian, Pavan Kumar, N., Min Zhong, Hu Yemin and Venugopal Reddy, P., "Structural, Magnetic and Dielectric Properties of $Bi_{0.9}Re_{0.1}FeO_3$ (Re = La, Sm, Gd and Y)", J Supercond Nov Magn 28, 2627, 2015.

Chapter 5

Conclusions

5.1 Conclusions

The present investigation has been focused on morphological, dielectric and magnetic properties of $Bi_{1-x}Gd_xMnO_3$ (x= 0.00-0.12) ceramics synthesized by conventional solid state reaction technique. The Gd substitution in place of Bi in $BiMnO_3$ ceramics significantly reduced the grain size up to ~200 nm with a narrow size distribution. However, due to the substitution of Gd the oxygen vacancies of all compositions were increased noticeably compared to undoped $BiMnO_3$. The Gd substitution also stabilized the dielectric constant at high frequencies by suppressing the low frequencies dispersion. In the Gd substituted $BiMnO_3$ ceramics the decreased grain size obviously increased the grain boundary and hence we have expected a higher dielectric constant. In reality, the dielectric constant was decreased due to the substitution of Gd in $BiMnO_3$. We think that the large oxygen vacancies generated in this ceramic system are responsible for reducing the dielectric constant. Due to the substitution of Gd, the magnetic parameters like remanent magnetization and coercivity were also increased at room temperature although the increment was nominal. In the undoped $BiMnO_3$, we have observed a ferromagnetic to paramagnetic transition at temperature around 45 K and below this phase transition temperature there was splitting between zero field cooled and field cooled magnetization curves. The substitution of 4 % Gd coincide the ZFC and FC magnetization curves along with a clear upturn of magnetization below the phase transition temperature. The steep increase of magnetization below phase transition temperature corresponds to the large magnetic contribution of Gd^{3+} (8 μB).

This investigation reveals that the optimum Gd concentration is 12%, to obtain better morphological, dielectric and magnetic properties.

5.2 Future Work

In this investigation, we have studied morphological, dielectric and magnetic properties at room temperature. It will be equally important to observe temperature dependent multiferroic properties of this material system. From temperature dependent magnetization experiments the exchange bias (EB) effect in this multiferroic system would be measured in details by varying cooling field and temperature, which may be useful in spintronic device applications.

The crystal structure plays an important role in the determining the magnetic states [1, 2], therefore, the pressure dependent magnetic properties of this ceramic system would be carried out in future investigation.

The preparation of nanoparticles of this material system would also be worthwhile using different physical and chemical techniques [3,4].

References:

[1] Sundaresan, A., Mangalam, R. V. K., Iyo, A., Tanaka, Y. and Rao, C. N. R., "Crucial role of oxygen stoichiometry in determining the structure and properties of $BiMnO_3$",   J. Mater. Chem. 18, 2191, 2008.

[2] Belik, A. A., Kolodiazhnyi, T., Kosuda, K. and Takayama-Muromachi, E., "Synthesis and properties of non-stoichiometric $BiMnO_3$", J. Mater. Chem. 19, 1593, 2009.

[3] Basith, M. A., Khan, F. A., Bashir Ahmmad, Shigeru Kubota, Fumihiko Hirose, Ngo, D.-T., Tran, Q.-H. andMølhave, K. "Tunable exchange bias effect in magnetic $Bi_{0.9}Gd_{0.1}Fe_{0.9}Ti_{0.1}O_3$ nanoparticles at temperatures up to 250K" J. Appl. Phys 118, 023901, 2015.

[4] Basith,M. A., Ngo,D.-T.,Quader,A.,Rahman,M. A.,Sinha,B. L. Bashir Ahmmad, FumihikoHirosedand Mølhaveb, K., "Simple top-down preparation of magnetic$Bi_{0.9}Gd_{0.1}Fe_{1-x}Ti_xO_3$ nanoparticles byultrasonication of multiferroic bulk material", Nanoscale6, 14336,2014.